remote sensing

MDPI

Article

Water Level Change of Qinghai Lake from ICESat and ICESat-2 Laser Altimetry

Weixiao Han [1], Chunlin Huang [1,*], Juan Gu [2], Jinliang Hou [1], Ying Zhang [1] and Weizhen Wang [1]

[1] Key Laboratory of Remote Sensing of Gansu Province, Heihe Remote Sensing Experimental Research Station, Northwest Institute of Eco-Environment and Resources, Chinese Academy of Sciences, Lanzhou 730000, China
[2] Key Laboratory of Western China's Environmental Systems, Ministry of Education, Lanzhou University, Lanzhou 730000, China
* Correspondence: huangcl@lzb.ac.cn

Abstract: Long-term satellite observations of the water levels of lakes are crucial to our understanding of lake hydrological basin systems. The Ice, Cloud, and Land Elevation satellite (ICESat) and ICESat-2 were employed to monitor the water level of Qinghai Lake in the hydrological basin. The median of absolute deviation (MAD) method was exploited to remove the outliers. The results confirmed that the MAD range of ICESat was from 0.0525 to 0.2470 m, and the range of σ was from 0.0778 to 0.3662 m; the MAD range of ICESat-2 was from 0.0291 to 0.0490 m, and the range of σ was from 0.0431 to 0.0726 m; ICESat-2 was less than that of ICESat. The reference ellipsoid and geoid transfer equations were applied to convert the water level to the World Geodetic System (WGS84) and Earth Gravitational Model 2008 (EGM2008) geoid. The water level, as derived from laser altimeters, was validated by the Xiashe Hydrological Station; with ICESat, the coefficient of association (R) was 0.8419, the root mean square error (RMSE) was 0.1449 m, and the mean absolute error (MAE) was 0.1144 m; with ICESat-2, the R was 0.6917, the RMSE was 0.0531 m, and the MAE was 0.0647 m. The water levels from ICESat-2 are much more accurate than those from ICESat. The two combined laser altimeters showed that the R was 0.9931, the RMSE was 0.1309 m, and the MAE was 0.1035 m. The water level rise was 3.6584 m from 2004 to 2020. The rising rate was 0.2287 m/a. The collaborative use of the ICESat-2 and ICESat satellites made it easier to obtain the lake water levels.

Keywords: Qinghai Lake; ICESat; ICESat-2; laser altimetry; water level

Citation: Han, W.; Huang, C.; Gu, J.; Hou, J.; Zhang, Y.; Wang, W. Water Level Change of Qinghai Lake from ICESat and ICESat-2 Laser Altimetry. *Remote Sens.* **2022**, *14*, 6212. https://doi.org/10.3390/rs14246212

Academic Editor: Pavel Kishcha

Received: 24 October 2022
Accepted: 6 December 2022
Published: 8 December 2022

1. Introduction

Surface water bodies sustain diverse, complex societies and ecosystems [1,2]. Lakes account for a substantial portion of the world's surface water bodies. They provide vital water resources for terrestrial ecosystems and are key components of the global hydrological basin system [3]. The water level is the most direct factor in the shrinkage and expansion of lakes. Tracking and quantifying lake water levels are challenging, particularly for alpine lakes [4]. Under the background of climate warming, natural factors, such as melting glaciers and increasing river runoff, along with human factors, such as dam construction and agricultural irrigation, have led to significant changes in lake water levels [5]. Therefore, verifying the water level derived from satellite data is a key and indispensable part of scientific research [6]. The water level of lakes has recently become a research topic of interest. These changes result from rapid climate change and cryosphere variations in the relevant region [7]. The lake water mass balance and the hydrological cycle could be established using the water level changes seen in lakes [8]. The mass variations in Iran were estimated using gravity applications; the main factor was groundwater [9]. The groundwater recharge zones in Ali Al-Gharbi District, Southern Iraq, were delineated using the multi-criteria decision-making model and Geographic Information Systems (GIS) [10].

The water level changes of lakes in the Tibetan Plateau (TP) offer a more sensitive indicator of climate change than lakes in other global regions [11]. The plateau, known as the 'Asian water tower', spans 3 million square kilometers across southern and central Asia, and its rivers provide water to more than 2 billion people [12]. The TP has the largest snow and ice mass in the world except for the Arctic and Antarctic regions. Many rivers and lakes are fed by these snow and ice masses [13,14]. Most of these lakes have experienced great changes over the past three decades and are still changing rapidly because of climate change. Previous research has shown that approximately 30 new lakes have appeared, whereas five existing lakes have dried up and faded in the period from 1975 to 2006 [14]. In addition, most of the 13 largest lakes (> 500 km^2) have experienced drastic changes. For example, Siling Co has expanded by 600 km^2, accounting for approximately 26% of the total area since 1976 [15], while the area of Qinghai Lake first decreased by 231 km^2 and then expanded by 134 km^2 from 1973 to 2013 [16]. Most of the lake basin systems in the TP are endorheic; Qinghai Lake is a classical endorheic lake in the TP [17]. Previous studies investigated changes in the lakes area in the TP by employing optical images from certain satellites, these images are restricted in terms of spatial and temporal seamless coverage due to frequent contamination from cloud cover and other unfavorable conditions. Therefore, it is essential to monitor the lake dynamics in the lake basin, especially the water level. To date, some studies on the water level changes in some lakes have been performed for the TP [18,19]. Water-level measurements obtained from satellite radar/laser altimetry have proven to be useful for monitoring inter-annual and intra-annual changes [20–22]. The water-level data available for lakes are often proprietary, inaccessible, or provided in idiosyncratic formats, especially in the case of remote alpine water bodies, most notably for the TP [23,24]. The most popular water-level-related databases are the United States Department of Agriculture Foreign Agricultural Service (USDA-FAS) global reservoir and lake monitoring database (GRLM; available at https://appliedsciences.nasa.gov/what-we-do/projects/global-reservoir-and-lake-monitor-grlm-expansion-and-enhancement-water-height (5 December 2022)), the database for the hydrological time series of inland waters (DAHITI, https://dahiti.dgfi.tum.de (5 December 2022)), HYDROWEB (http://hydroweb.theia-land.fr (5 December 2022)), and the global reservoirs and lakes monitor (G-REALM, https://ipad.fas.usda.gov/cropexplorer/global_reservoir (5 December 2022)).

Water level changes in lakes have traditionally been derived from hydrological station data. The hydrological station data can provide precise daily water-level observations. The in situ water level datasets, however, are often time-consuming and expensive to obtain. This is particularly true in remote and alpine areas where no routinely gauged water-level measurements are available [25–27]. The water-level fluctuations of Lake Urmia were monitored and assessed using the multitemporal Landsat 7 [28]. Meanwhile, the water-level fluctuations of Lake Nasser were monitored using Landsat 8, Jason-2, and Jason-3 [29]. Satellite radar altimetry has been widely used to monitor changes in lake levels [22,30–39]. Although radar altimeters can track water levels from space, the large footprints used (~1–10 km) and the sparse along-track (0.3–7 km)/cross-track (80–300 km) spacing limit their applicability for continuous observation [33]. Laser altimetry has revealed a higher performance than radar altimetry, including the Ice, Cloud, and Land Elevation satellite (ICESat) and ICESat-2 [40,41]. Its small footprint size, with a diameter of about 70 m, is one of the greatest advantages of ICESat laser altimetry, enabling the measurement of the elevations of the earth's surface on a fine scale [40]. For ICESat, the results of Qinghai Lake showed that the mean water level rose 0.67 m during the period of 2003–2009, with an increase rate of 0.11 m/a, and that the water level correlated well with the gauge measurements (r^2 = 0.90, where the root mean square difference equals 0.08 m) [18]. The ICESat-2 mission followed the ICESat, by which means sustained, high-accuracy observation has been provided. The ICESat-2 operated after 2018 and provided information on inland water elevations, sea surface heights, land and vegetation heights, cloud layering and optical thickness, and mountain glacier and ice cap elevation changes [41]. However, validation of the ICESat and ICESat-2 data is insufficient; meanwhile, the EGM2008 geoid and WGS84 reference ellipsoid must be applied to each ground track to facilitate comparison of long-term water level changes.. Therefore, it is crucial to evaluate the accuracy of the ICESat and ICESat-2 elevation measurements. It is also essential to evaluate the potential presence of bias between ICESat and ICESat-2 before undertaking a synthesized analysis. In this study, the change in water level in Qinghai Lake from the satellite data was studied, with the water level derived from ICESat and ICESat-2 data. The median of absolute deviation (MAD) outlier removal method was adopted, the geoid and ellipsoid reference were transferred, and the performance of ICESat and ICESat-2 in terms of lake water level was evaluated using gauge-based data.

Section 2 expounds upon the study area and dataset. Section 3 presents the methods, including the reference ellipsoid and datum transform and the outlier removal method. Section 4 illustrates the results of the EGM2008 geoid and ellipsoid transfer of ICESat and the outlier removal and validation of ICESat and ICESat-2. Section 5 discusses the different reference ellipsoids and geoids, the MAD outlier removal method, and the six ground tracks of ICESat-2. Section 6 offers our conclusions.

2. Study Area and Data

2.1. Study Area

Qinghai Lake is the largest lake on the Qinghai-Tibetan Plateau (QTP) in China. It is a brackish endorheic lake, located in the northeastern QTP, and is one of the 12 sub-basins of the QTP [42–44]. The watershed boundaries and free-flowing river network data were drawn from HydroSHEDS (https://www.hydrosheds.org/applications/free-flowing-rivers (5 December 2022)), while the surface water was established using the JRC global surface water mapping layers (https://global-surface-water.appspot.com/download (5 December 2022)) (Figure 1). Qinghai Lake (36.53°–37.25° N, 99.60°–100.78° E) has a surface water area of 4500 km^2; the average depth of the lake is 21.0 m, and the maximum is 32.8 m; it has a water volume of 7.16 × 1010 m^3 [42,45–49]. The lake formed because of the development of a fault depression between the Qilian Mountains, the Qinghai Nanshan, and the Riyue Mountains, and has an elevation of 3194 m a.s.l. [50,51]. The lake is currently fed by several rivers, with a total water discharge of 1.56 × 109 m^3 [52]. Over the past 57 years, the annual average temperature was 1.9 °C [51]. The mean temperatures of the most recent 40 years were −11.4 °C and 12.5 °C in January and July, respectively [10]. Qinghai Lake enters the ice period in about November; a stable ice sheet begins to form in December, and thawing begins in March or April [53–55].

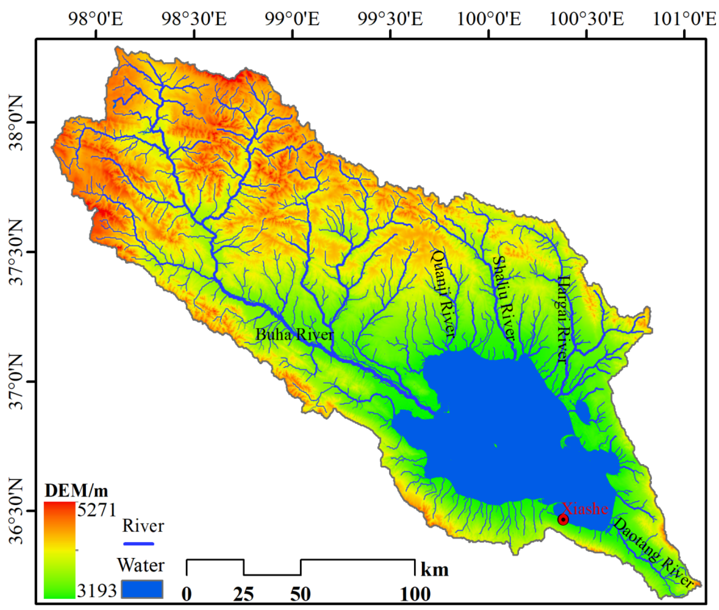

Figure 1. The location of Qinghai Lake.

2.2. Data

2.2.1. ICESat

ICESat was designed to measure ice-sheet mass balance, land topography and vegetation characteristics, and cloud and aerosol heights through time. It ran as part of the National Aeronautics and Space Administration's (NASA) earth-observing system (EOS). The sole instrument on ICESat was the geoscience laser altimeter system (GLAS), a space-based laser-ranging system (LiDAR). The GLAS emitted infrared and visible laser pulses at 1064 and 532 nm wavelengths and produced approximately 70-meter-diameter laser spots, separated by nearly 170 m along the ground track. The ground track took eight days during the mission's commissioning phase, then the satellite was maneuvered into a 91-day repeating ground track after August 2004 [40]. ICESat was launched on 13 January 2003, then the satellite was retired on February 2010. Products include the GLAS/ICESat L2 global land surface altimetry data; this level-2 altimetry product (GLAH14) provided the surface elevations for land (the data are available in the National Snow and Ice Data Center (NSIDC) (https://nsidc.org/data/GLA14/versions/34 (5 December 2022)), for which the account ID and password were requested. The high accuracy of the elevation measurements of ICESat in good weather conditions has been confirmed in previous studies [18,20,21,56–58]. The precision of the mean surface elevation of flat surfaces is ~2 cm [59,60]. ICESat elevation data over the water surface/flat surfaces in east Africa, southern Egypt, and the USA have been examined in numerous studies and have shown an accuracy of better than 10 cm [61–64].

2.2.2. ICESat-2

ATLAS/ICESat-2 L3A inland water surface height data were released in 2019 [65]; detailed information on observatory and ATLAS data is provided in Table 1. ICESat-2 collects elevation data over all the world's surfaces, from pole to pole. Products are available through the NSIDC. ATL13 is the inland water height product and includes lakes, estuaries, and rivers (https://nsidc.org/data/atl13/versions/5 (5 December 2022)). Detailed algorithmic steps are required to retrieve these products [66]. The ICESat-2 mission has a geolocation accuracy that is better than 6.5 m and the vertical accuracy is better than 10 cm [67]. The ground elevation accuracy of ICESat-2 was verified in Alaska, USA, while the overall mean difference and RMSE values between the ground elevations retrieved from the ICESat-2 data and the airborne LiDAR-derived ground elevations were −0.61 m and 1.96 m, respectively [68]. The data are available on the associated website https://openaltimetry.org/data/icesat2/ (5 December 2022)).

Table 1. The introduction of information on ICESat-2 mission parameters Reprinted with permission from Ref [41]. 2019, Neumann et al.

Orbit Inclination	92°	Coverage	Up to 88°N and S
Pointing control ATLAS	45 m	Pointing knowledge	6.5 m
Laser wavelength	532 nm	Number of beams	6 beams organized in 3 pairs
Pulse repetition rate	10 kHz (~0.7 m along-track spacing at nominal altitude)	Beam spacing (across-track) at nominal altitude	90 m within pairs; 3.3 km between pairs

2.2.3. Hydrological Station

The in situ daily water level values were sourced from the Xiashe Hydrological Station (36.58°N, 100.48°E), which is located in Xiashe Village, Gonghe County, Hainan Tibetan Autonomous Prefecture, Qinghai Province. The station is managed and operated by the Qinghai Hydrological and Water Resources Survey Bureau. The water-level dataset was provided by the Data Center for Eco-Environment Protection in the Qinghai Lake Basin (http://qhh.qhemdc.cn/ (5 December 2022)) [69].

The measured water-level data refer to the 1985 National Elevation Datum, launched on 1 January 1988. We calculated the elevation data, based on the tidal observation data from the Qingdao Tide Gauge Station from 1952 to 1979, and obtained the multiyear average sea level as the unified base surface area. The 1985 national elevation benchmark in the Qinghai Lake area was about 0.4000 m lower, according to a combination of reference points and site observations [70]. We obtained the specific difference by fitting and calculating the vertical deviation in China, using the polynomial approximation method [71]. The polynomial formula is as follows:

$$C = a_0 + a_1 dB + a_2 dL + a_3 dB^2 + a_4 dL^2 + a_5 dBdL \quad (1)$$

where $a_0 = 0.3572$, $a_1 = 0.0094$, $a_2 = 0.0012$, $a_3 = -0.0009$, $a_4 = 0.0002$, and $a_5 = 0.0014$; dB and dL are the differences between the longitude and latitude of the research site relative to the 1985 national elevation reference point, the Qingdao Tide Gauge Station. The geographic location of the Qingdao Tide Gauge Station, which was the national elevation reference point in 1985, is at 120°19′08″E, 36°04′10″N. The geographic location of the Xiashe Hydrological Station in Qinghai Lake is at 100°30′E, 36°35′N. We calculated that the Xiashe Hydrological Station was 0.402 m lower than the 1985 national elevation reference point.

2.2.4. Land/Water Mask

The MOD44W V6 land/water mask 250 m product provides the land/water mask data source. We applied a land/water mask derived from MODIS to address the boundaries of the water body. The spatial resolution is at 250 m, the temporal resolution is for one year, and the dataset availability was from 2000 to 2015. The water mask was evaluated by the water_mask_QA band, while the bitmask for quality assurance included 10 classes. The NASA Land Processes Distributed Active Archive Center (LP DAAC) provides datasets at the United States Geological Survey (USGS) Earth Resources Observation and Science (EROS) Center [72].

Meanwhile, the JRC yearly water classification history dataset, v1.4, represents the second land water mask data source; the spatial resolution is 30 m and the temporal resolution is one year. This dataset contains maps of the location and temporal distribution of surface water from 1984 to 2021. The boundary of the water body is enough to replenish MOD44W V6.

2.2.5. NASADEM

The NASADEM (released in February 2020) was created by reprocessing the Shuttle radar topography mission (STRM) radar data and merging it with other improved-accuracy DEM datasets, such as the Advanced Space-borne Thermal Emission and Reflection Radiometer (ASTER) Global Digital Elevation Map (GDEM), ICESat GLAS, and the panchromatic remote sensing instrument for stereo mapping (PRISM) datasets. The most significant processing improvements involved void reduction via improved phase unwrapping and used the ICESat GLAS data for control. The spatial resolution was 30 m. The dataset was provided by the NASA USGS JPL, Caltech [73].

3. Methodology

3.1. ICESat

3.1.1. ICESat Reference Ellipsoid and Datum Transform

ICESat/GLAS products give the latitude, longitude, and elevation along the track on a reference ellipsoid, which is the same as for the TOPEX/Poseidon and Jason-1 products. The equatorial radius was 6,378,136.300000 m, the polar radius was 6,356,751.600563 m, and the reciprocal flattening (1/f) was 298.257. Table 2 summarizes the differences between the reference ellipsoid used by ICESat/GLAS and the WGS84 reference ellipsoid.

Table 2. The parameters for the reference ellipsoids of ICESat/GLAS, CGCS2000, and WGS84.

Parameters	ICESat/GLAS	CGCS2000	WGS84
Equatorial radius (a)	6,378,136.300000 m	6,378,137.000000 m	6,378,137.000000 m
Polar radius (b)	6,356,751.600563 m	6,356,752.314140 m	6,356,752.314245 m
Reciprocal flattening (1/f)	298.25700000	298.257222101	298.25722356
Eccentricity (e)	0.081819221456	0.0818191910428	0.081819190843

For these products, the same location on Earth yields different reference ellipsoids to represent the three-dimensional coordinate points, which causes slight differences in the three-dimensional coordinate points. The difference between the latitude and longitude of the Earth produced a horizontal offset of less than 1 m. Because the horizontal offset was much smaller than the positioning accuracy of GLAS in the horizontal position, it could be ignored. The difference was mainly in the elevation of the earth. The ICESat/GLAS reference ellipsoid was about 0.70 m smaller than the WGS84 reference ellipsoid. Therefore, the elevation measured using the ICESat/GLAS reference ellipsoid was higher than the elevation measured using the WGS84 reference ellipsoid (https://nsidc.org/sites/default/files/glas-atbd-laserfootprintlocation28geolocation2926surfaceprofiles-v12-jul2014.pdf (1 July 2014)). The calculation formula for the elevation difference is as follows:

$$\Delta\_h = h2 - h1 = -((a2 - a1) \times (\cos(phi))^2 + (b2 - b1) \times (\sin(phi))^2 \quad (2)$$

where phi is the latitude; h1 and h2 are the geodetic elevations, measured by reference ellipsoid 1 and ellipsoid 2, respectively; a1 and a2 are the equatorial radii measured by reference ellipsoid 1 and ellipsoid 2, respectively; and b1 and b2 are the polar radii measured by reference ellipsoid 1 and ellipsoid 2, respectively. The latitude range of Qinghai Lake is 36.5333°–37.2500°N. We calculated the range of elevation difference between the reference ellipsoids of ICESat/GLAS and WGS84 as −0.7116 to −0.7026 m and calculated the average value of −0.7071 m as the conversion value of the elevation difference between the two reference ellipsoids. Due to the irregular geometrical shape of Qinghai Lake, the mean value calculated here is only calculated according to the maximum and minimum values. Each track and its sub-satellite point should have a corresponding reference ellipsoid and elevation datum conversion value that is replaced by the mean value, which has a certain uncertainty.

The ICESat/GLAS data products use the EGM96 geoid to obtain more accurate elevation data. We used the EGM2008 geoid data along the track in the ICESat-2 and calculated the EGM2008 geoid gridded data with a spatial resolution of 0.01° in the Qinghai Lake region (99.60°–100.77°E,36.53°–37.25°N), using the inverse distance weighting method. The spatial resolution of 0.01° is about 1 km, while the along-track resolution is 170 m (40 Hz), the footprint is 50–90 m, and the uncertainty is at this location [64]. The datum transform formula of ICESat is as follows:

$$ICESat\_WGS84\_EGM2008 = ICESat\_Topex - EGM2008 - D\_Topex\_WGS84 \quad (3)$$

where ICESat_Topex is the elevation of the ICESat with TOPEX/Poseidon reference ellipsoid; EGM2008 represents the grid data with a spatial resolution of 0.01° in the Qinghai Lake region; and D_Topex_WGS84 is the difference between the TOPEX/Poseidon reference ellipsoid and *WGS84* reference ellipsoid, which is 0.7071 m.

3.1.2. ICESat Preprocessing

The ICESat along track passed over Qinghai Lake, where six tracks were recorded. Figure 2 shows the track ID and the corresponding number of days: the track IDs were 1239, 1306, 376, 443, 71, and 4; the corresponding number of days was 1, 16, 13, 1, 3, and 13; the total number of days was 47. Table 3 presents the tracks and their corresponding dates according to the track order, from right to left. Figure 3 shows the elevation variation along the track, according to latitude. Obviously, because of the influence of the terrain around the lake, the elevation around the lake changed significantly, and the elevation was higher than the elevation of the lake's surface. Some outliers still existed in the ground along the track, and these values interfered with the measurement of lake levels, with the elevation of the lake surface being the lowest value. Therefore, we processed these values further and removed the outliers.

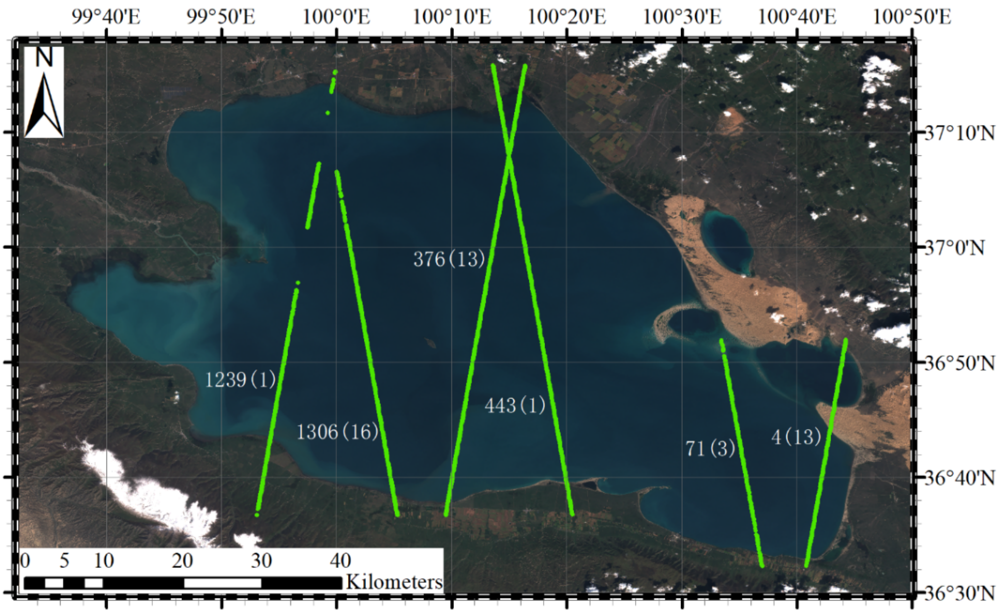

Figure 2. The track ID and the corresponding number of days of the ICESat along-track pass over Qinghai Lake (note: this figure is created using Sentinel-2 data).

Table 3. The track ID and its corresponding dates for the ICESat along-track pass over Qinghai Lake.

Track (Days)	Date	Track (Days)	Date	Track (Days)	Date
1306 (16)	18/10/2003	1239 (1)	14/10/2003	71 (3)	27/02/2008
	19/02/2004	376 (13)	16/11/2003		14/10/2008
	20/05/2004		18/03/2004		18/03/2009
	06/10/2004		17/06/2004	4 (13)	22/10/2003
	20/02/2005		03/11/2004		22/02/2004
	22/05/2005		21/11/2005		24/02/2005
	23/10/2005		24/03/2006		26/05/2005
	24/02/2006		23/06/2006		27/10/2005
	26/05/2006		24/2112006		27/02/2006
	27/10/2006		11/04/2007		29/05/2006
	13/03/2007		02/11/2007		30/10/2006
	04/10/2007		18/03/2008		17/03/2007
	19/02/2008		14/12/2008		08/10/2007
	06/10/2008		08/04/2009		22/02/2008
	10/03/2009	443 (1)	08/11/2004		09/10/2008
	02/10/2009				14/03/2009

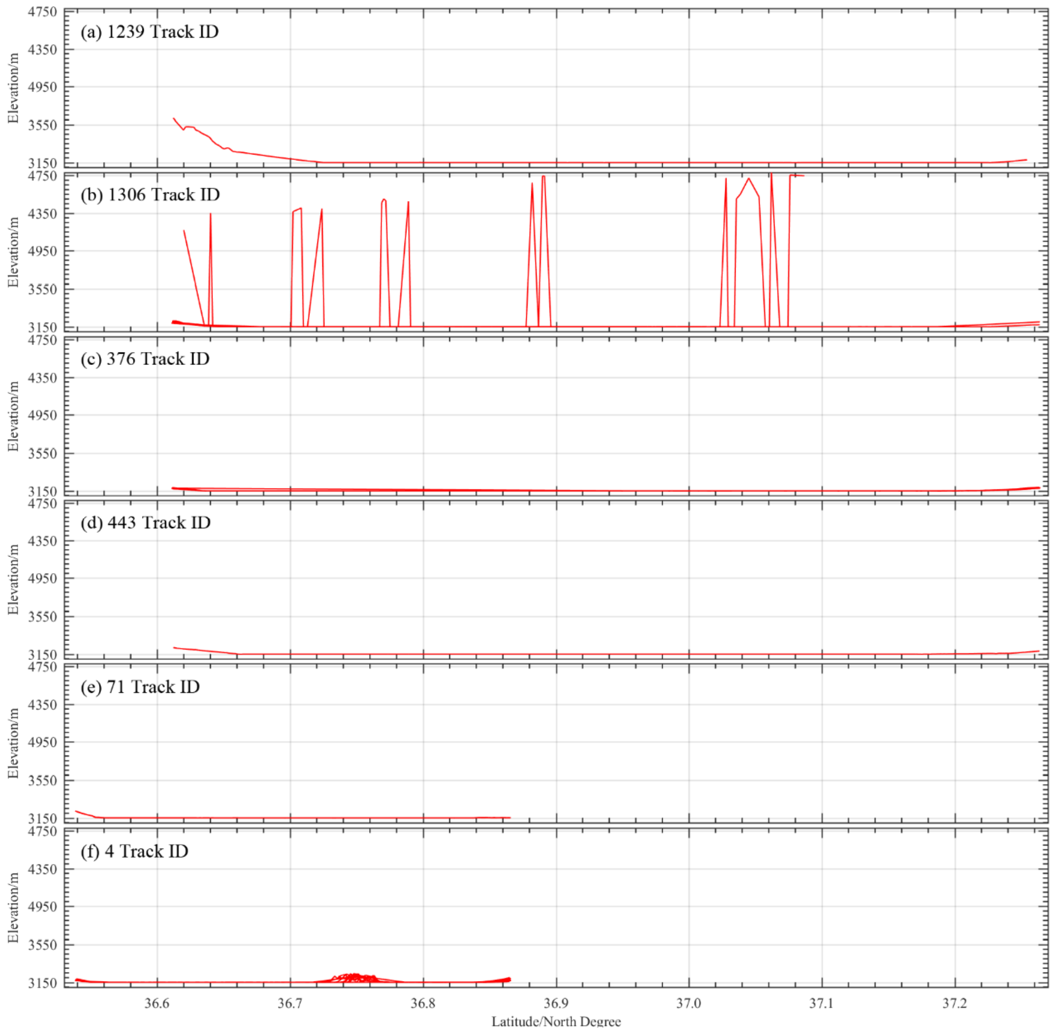

Figure 3. The elevation variation along the latitude in each track of ICESat.

3.2. ICESat-2

3.2.1. ICESat-2 Reference Ellipsoid and Datum

The water surface heights of ICESat-2 are provided as both the height above the WGS 84 reference ellipsoid and the height above the EGM2008 [41,74]. This is consistent with the result of the ICESat reference ellipsoid and datum transform, to facilitate combination and comparison with the in-situ water-level data.

3.2.2. ICESat-2 Preprocessing

The IDs of the track beams of the ICESat-2 that passed over Qinghai Lake were 568, 652, 1010, 1094, 65, 149, 507, and 591, and had a total of eight reference ground tracks (RGTs). The track beams and their overflight days are shown in Figure 4. The track IDs and the corresponding dates are presented in Table 4, and the number of available days was 43 days. Six beams, configured in a 2 $\times$ 3 array (three pairs), passed over Qinghai Lake. The data time period ranged from 31 October 2018 to 5 July 2020. Figure 5 shows the elevation variation along the track, according to latitude. Obviously, the elevation in the middle of track IDs 568 and 652 was higher than the elevation of the lake surface because of the influence of the terrain around the lake. The six beams in each track have been considered as one track. In addition, outliers also had a certain influence on the water level. Some outliers existed in the ground along the track, especially in track IDs 507 and 591. These values interfered with the measurement of the lake level, and the elevation of the lake surface was the lowest value. Therefore, we processed these values further and removed the outliers.

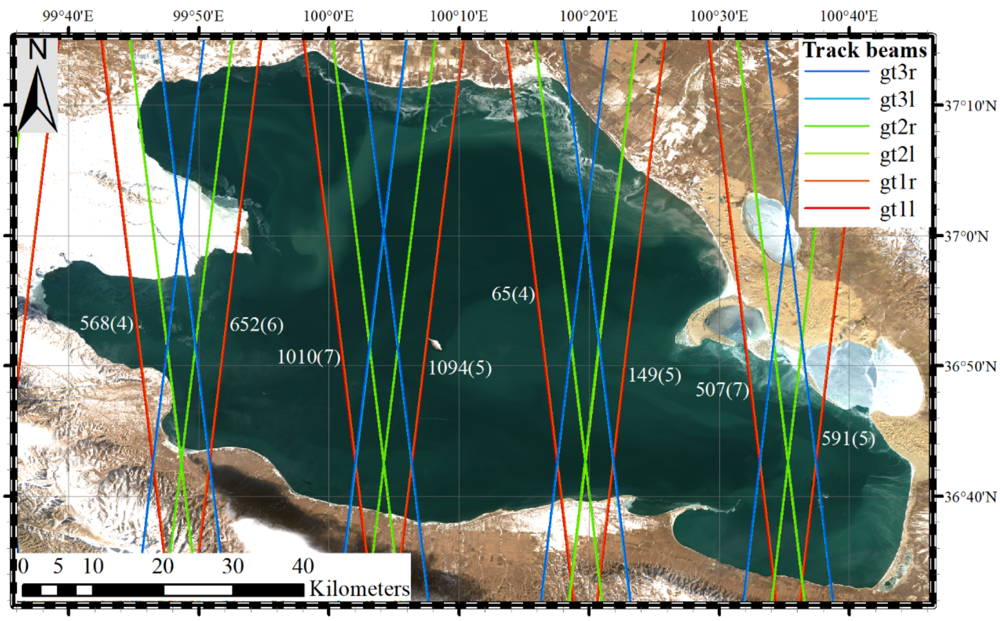

Figure 4. The track beams of the ICESat-2 overpass of Qinghai Lake (note: Landsat 8 Operational Land Imager (OLI) from 10 December 2018).

Table 4. Track IDs and the corresponding available days of ICESat-2 data covering Qinghai Lake.

Track (Days)	Date	Track (Days)	Date	Track (Days)	Date
568 (4)	03/02/2019	1094 (5)	10/03/2019	507 (7)	31/10/2018
	04/08/2019		07/09/2019		30/01/2019
	03/11/2019		07/12/2019		01/05/2019
	02/05/2020		07/03/2020		31/07/2019
652 (6)	10/11/2018		06/06/2020		30/10/2019
	09/02/2019	65 (4)	01/01/2019		28/01/2020
	10/05/2019		01/10/2019		28/04/2020
	09/08/2019		30/12/2019	591 (5)	05/02/2019
	08/11/2019		29/06/2020		05/08/2019
	07/02/2020	149 (5)	07/01/2019		04/11/2019
1010 (7)	03/12/2018		06/10/2019		03/02/2020
	04/03/2019		05/01/2020		04/05/2020
	03/06/2019		05/04/2020		
	02/09/2019		05/07/2020		
	02/12/2019				
	01/03/2020				
	31/05/2020				

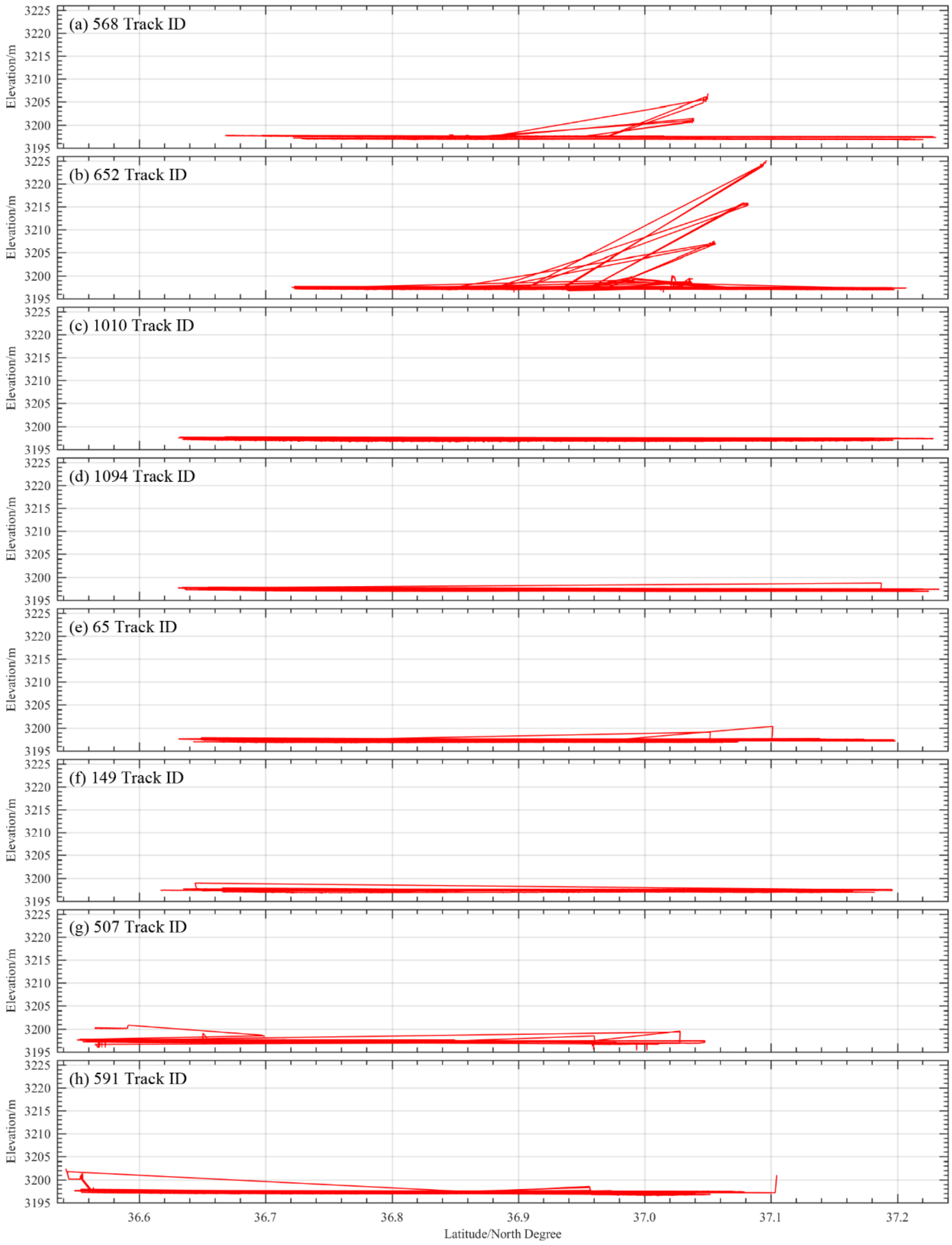

Figure 5. The elevation variation along the latitude in each track of ICESat-2.

3.3. *Reference Ellipsoid and Datum Transform of Hydrological Station*

The water level of the Xiashe hydrological station is referenced as the 1985 national elevation benchmarks (EPSG:5737) datum and the China Geodetic Coordinate System 2000 (CGCS2000, EPSG:5737) as the reference ellipsoid [75]. Table 2 presents the parameters. Since the parameters of the two reference ellipsoids are the same, the difference in latitude, longitude, and elevation of the Earth can be ignored. Because the 1985 national elevation benchmarks of 0.2980 m and 0.4642 m were above the mean sea level and the global geoid, we added the elevation values to two offsets.

Therefore, it was critical to convert the local hydrological water level, based on the 1985 national elevation benchmarks to a unified reference ellipsoid. The 1985 national elevation benchmarks that are currently adopted represent a local elevation datum. The zero for water level is the water level of the tide gauge station in the Yellow Sea (120°19′08″E, 36°04′10″N) in 1985, and the location of the Xiashe Hydrological Station is 100°30′E, 36°35′N. The polynomial approximation method fits the vertical deviation in a different location in China [71]. The polynomial is expressed as follows:

$$C = a_0 + a_1 dB + a_2 dL + a_3 dB^2 + a_4 dL^2 + a_5 dBdL \quad (4)$$

where $a_0 = 0.3574$, $a_1 = 0.0094, a_2 = 0.0012, a_3 = -0.0009, a_4 = 0.0002$, and $a_5 = 0.0014$.

The deviation between the Xiashe Hydrological Station and the 1985 national elevation benchmark tide gauge station was 0.4022 m.

On the basis of this difference, the water level of the Xiashe Hydrological Station was transformed, using the following equation:

$$\text{In\_situ\_T} = \text{In\_situ} + \text{D\_Sta\_1985} + \text{A\_geoid} + \text{A\_msl} \quad (5)$$

where In_situ is the in situ water level; D_Sta_1985 is the elevation difference between the Xiashe Hydrological Station and the 1985 national elevation benchmark tide gauge station; A_geoid is the elevation value by which the 1985 national elevation benchmarks are higher than the global geoid; A_msl is the elevation value by which the 1985 national elevation benchmarks are higher than the mean sea level; D_Sta_1985 = 0.4022 m; A_geoid = 0.4642 m; and A_msl = 0.2980 m. Due to the large area of Qinghai Lake, the site of the water level data of Xiashe Hydrological Station is located on the shore of Qinghai Lake. Therefore, it is not possible to use the water level data of Xiashe Hydrological Station to validate the remote sensing water level data of ICESat and ICESat-2 in terms of spatial representativeness.

3.4. Outlier Removal

To filter the outliers in each track, we combined the elevation values of all days on the same track. Because of the lake's surface elevation characteristics and its surrounding terrain, the lake's surface elevation was at its lowest point. Those values that were higher than the median, plus a threshold, were excluded. We implemented an alternative and robust measure of dispersion (i.e., MAD) [76–78] to measure the central tendency, which had the advantage of being insensitive to the outliers, especially the extreme values. We calculated MAD as follows: (1) the median of all series elevations of all days in the same track was calculated, where M = median (elevation); (2) the series of absolute deviations between all series elevations and the median (M) value were calculated, where AD = abs (elevation−M); (3) the median of AD was calculated, where MAD = median (AD); (4) the threshold was calculated, where σ = 1.4826 MAD; (5) the filter criteria were defined, where the area outside of the range [M + 3σ, M−3σ] was excluded.

In addition, the elevation derived from the ICESat included the land surface elevation and lake surface elevation. Therefore, to eliminate the effect of the land surface and the coastal contamination, it was necessary to preprocess the elevation of ICESat before the filter outlier processes. It was critical to exclude the land surface elevation for the ICESat; 47 overflights of ICESat were available over Qinghai Lake, and there were six tracks. We used the minimum boundary of Qinghai Lake in 2004 to remove the land surface and coastal surface elevations.

4. Results

4.1. ICESat

4.1.1. ICESat Outlier Removal

We used the annual water mask boundary to remove the influence of terrain and to retain the orbital laser elevation data of the lake's interior. Due to the vast extent of Qinghai Lake, surface waves on the lake surface result from wind interactions, and so the water level along the ground track is constantly changing. There were sudden changes in the water levels of some adjacent positions in each track. Furthermore, the MAD outlier method was used to remove the outlier values from the ground track. Table 5 presents the parameters of the MAD outlier method in each of the combined tracks, for which the deviation of water surface height in each track of ICESat is shown. The median values were around 3150.0000 m; the range of MAD was from 0.0525 to 0.2470 m and the deviation of the water surface height in each track of ICESat was small; the range of σ was from 0.0778 to 0.3662 m, and the corresponding range of [M + 3σ, M−3σ] closely surrounded the MAD. The minimum value was slightly less than the median, but the maximum value was much larger than the median. Table A1 presents the parameters of the MAD outlier method, with the corresponding daily dates. Figure 6 shows the elevation variation along the latitude in each track of ICESat, using the water mask boundary and the MAD outlier method. It was the obvious choice to count the number of days that each track covered, which corresponded exactly to the numbers shown in Figure 2. The water level of Qinghai Lake was about 3194 m. A certain disparity between the water level of Qinghai and that recorded by ICESat was the result of differences in the ICESat reference ellipsoid and the elevation datum. Therefore, we converted the water level data from the reference ellipsoid and elevation datum to the WGS84 reference ellipsoid and the EGM2008 geoid.

Table 5. The statistical parameters of the MAD outlier method used in each combined track.

Track	M/m	MAD/m	σ/m	M-3σ/m	M+3σ/m	Min/m	Max/m
4	3150.5050	0.1200	0.1779	3149.9713	3151.0387	3147.7580	3158.2440
71	3150.3450	0.2470	0.3662	3149.2464	3151.4436	3149.7200	3153.7340
376	3149.7020	0.1600	0.2372	3148.9904	3150.4136	3148.0560	3155.9920
443	3149.4660	0.0525	0.0778	3149.2326	3149.6994	3148.1810	3152.5440
1239	3149.3610	0.1040	0.1542	3148.8984	3149.8236	3148.5610	3153.1570
1306	3149.6570	0.2470	0.3662	3148.5584	3150.7556	3147.7000	4781.5790

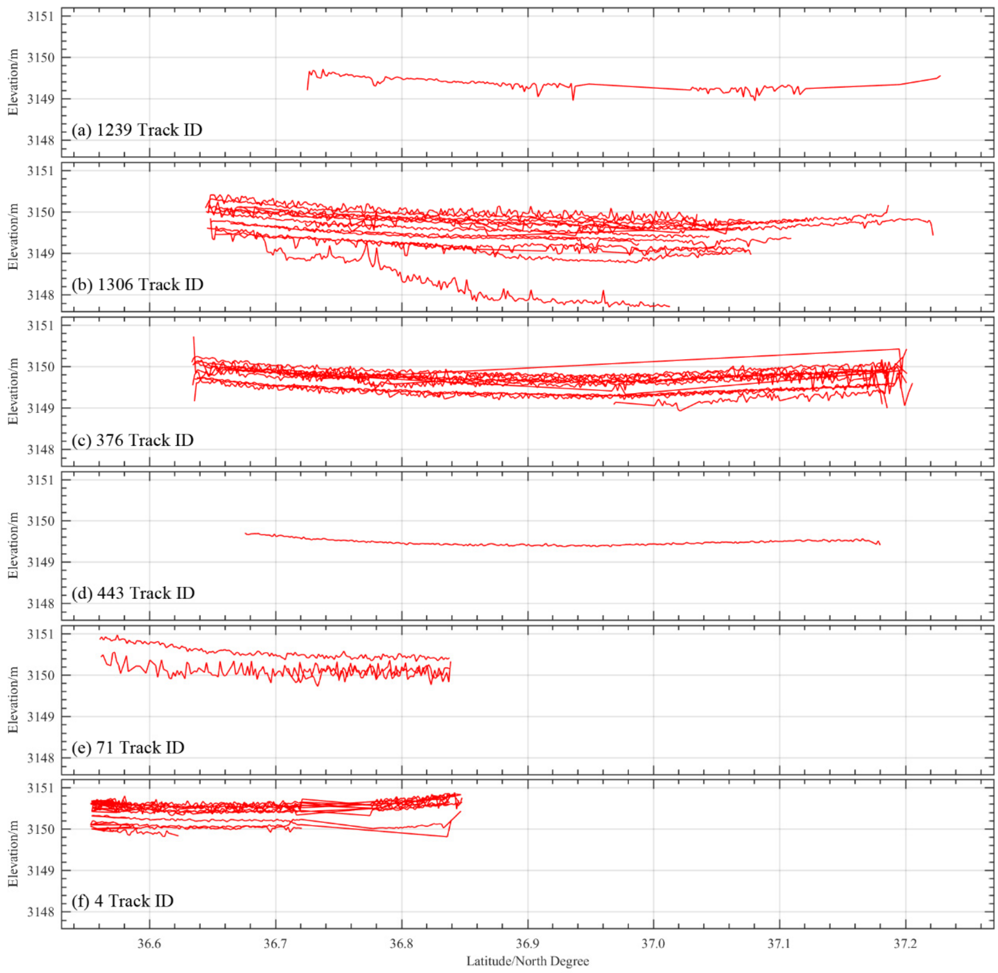

Figure 6. The elevation variation along the latitude in each track of ICESat, using the water mask boundary and the MAD outlier method.

4.1.2. ICESat EGM2008 Geoid and Ellipsoid Transfer

To unify the reference ellipsoid and the elevation datum, we used Equations (2) and (3) to convert the water level of ICESat to the EGM2008 geoid and WGS84 reference ellipsoid. Figure 7 shows the elevation variation according to latitude in each track of ICESat, using the EGM2008 geoid and the WGS84 reference ellipsoid. The water level that was derived from ICESat was about 3194 m, and the water level values oscillated up and down with the nearby mean value. On the same track, the variation in the water level on different dates could be distinguished, which also reflected the changes in water levels on different days.

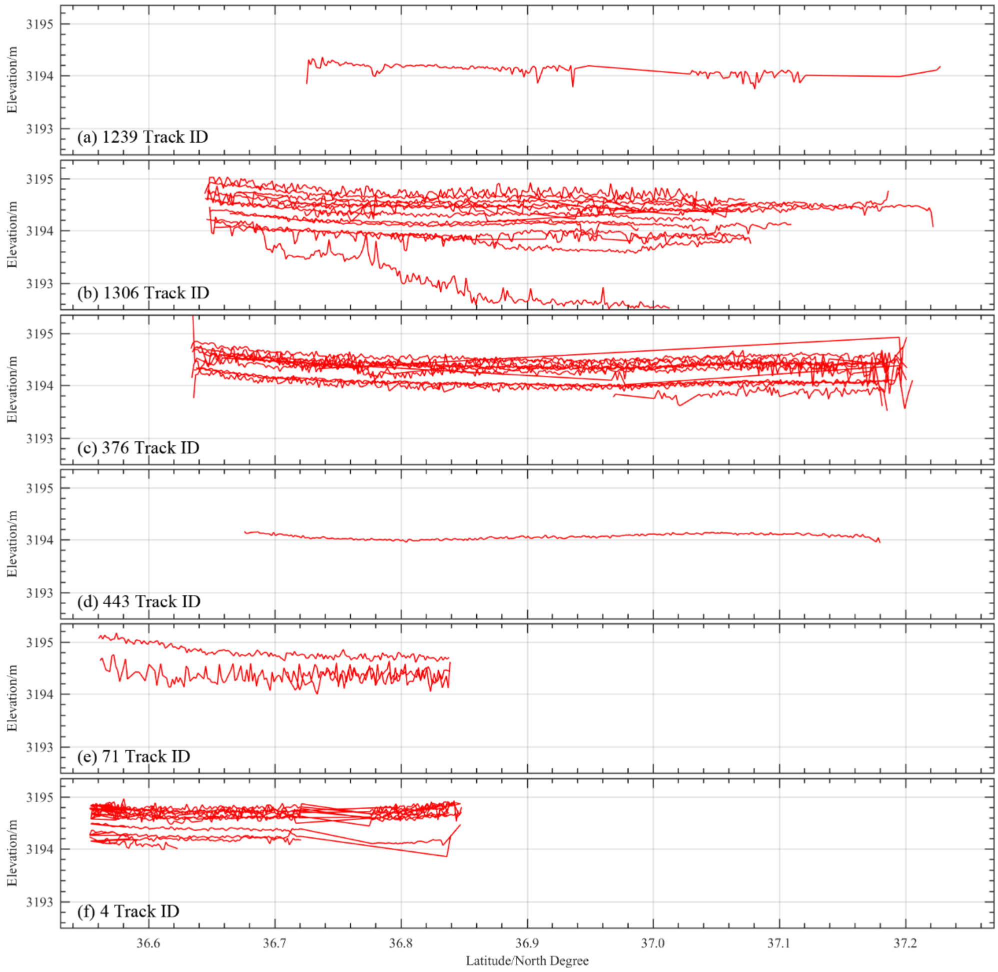

Figure 7. The elevation variation along the latitude in each track of ICESat, using the EGM2008 geoid and WGS84 reference ellipsoid.

4.1.3. Validation of ICESat

To validate the accuracy of the water-level data of ICESat, we used the in situ water level derived from the Xiashe Hydrological Station and applied Equation (4) to compensate for the vertical deviation in a different location in China. We used Equation (5) to convert the water level to the EGM2008 geoid. Table A2 presents the matched validation results for ICESat, using the Xiashe Hydrological Station; the first column is the date, the second column is the water level, derived from ICESat, the third column is the in situ water level, derived from the hydrological station, and the fourth column is the bias of the water level (ICESat—in situ). We obtained a total of 47 validation points. The maximum absolute bias value was −0.9622 m, which was recorded on 20 May 2004. Figure 8 shows the scatter diagram of the validation results of the ICESat using the in situ water level. The R (correlation coefficient) value was 0.7969, the root mean square error (RMSE) was 0.2024 m, the mean absolute error (MAE) was 0.1325 m, and the mean error (ME) was −0.0034. One of the matched points was further away from the 1:1 line; the date ID was 20 May 2004 and the preceding and the following two date IDs were 18 March 2004 and 17 June 2004, respectively, and the water levels were 3193.8656 m and 3194.0195 m, which values were close to the in situ water level. These results were quite different from the water level on the preceding and the following dates. In particular, this level was different from the in situ water level. Therefore, we removed this point under the validation results for the ICESat data, following which the MAE dropped to 0.1144 m, the RMSE dropped to 0.1449 m, and the R increased to 0.8419.

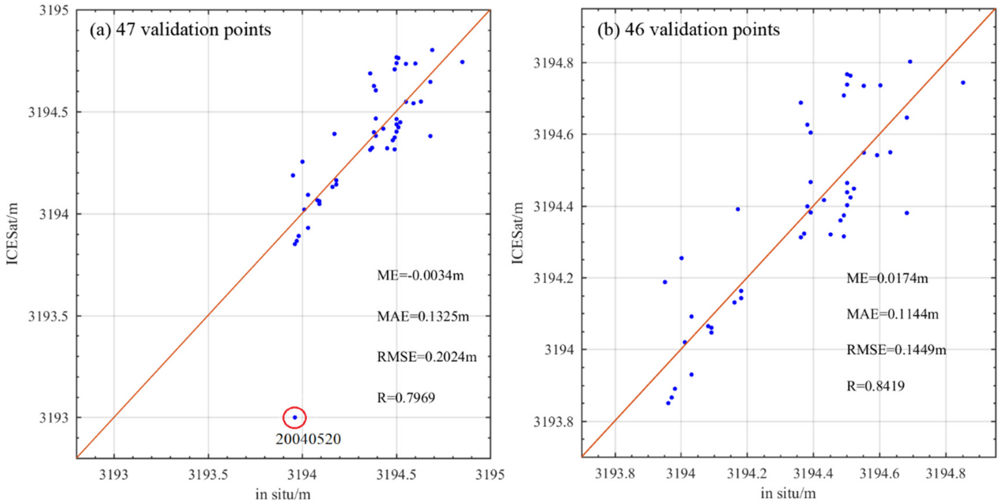

Figure 8. The validation results of the ICESat using the in-situ water level: (**a**) the total validation points, red circle represents abnormally deviated scattered point; (**b**) 46 validation points with one point excluded).

4.2. ICESat-2

4.2.1. ICESat-2 Outlier Removal

We used the same methods for the water level values derived from ICESat-2. We used the annual water mask boundary to remove the influence of terrain and retained the orbital laser elevation data of the lake's interior. Furthermore, we used the MAD outlier method to remove the outlier values of the ground track. Table 6 presents the parameters of the MAD outlier method in each combined track; the deviation of water surface height in each track of ICESat-2 is also shown. The median values were around 3197.3133 m, which was around 2.8 m higher than that of the ICESat values. The range of MAD was from 0.0291 to 0.0490 m, which was less than that of ICESat (0.0525 to 0.2470 m), and the deviation of water surface height in each track of ICESat-2 was smaller. The range of σ was from 0.0431 to 0.0726 m, and the corresponding range of [M + 3σ, M-3σ] closely surrounded the MAD range. The minimum value was slightly lower than the median, but the maximum value was larger than the median (some were significantly larger than the median). Table A3 presents the parameters of the MAD outlier method, with the corresponding daily dates. We combined the six beams as one ground track and used the daily MAD parameters for the water level of the corresponding daily dates. Figure 9 shows the elevation variation along the six beams of one track according to latitude, using the water mask boundary and the MAD outlier method. It was the obvious choice to depict the six beams of all tracks. Because the six beams of each track changed slightly, those beams were woven together in a sort of skein. This corresponded exactly to the six numbers shown in Figure 4.

Table 6. The statistical parameters of the MAD outlier method in each combined track.

Track	M/m	MAD/m	σ/m	M-3σ/m	M+3σ/m	Min/m	Max/m
65	3197.3131	0.0319	0.0472	3197.1714	3197.4548	3196.7197	3200.3542
149	3197.3088	0.0307	0.0455	3197.1723	3197.4453	3196.7236	3198.9220
507	3197.3135	0.0354	0.0525	3197.1560	3197.4710	3195.3083	3200.8225
568	3197.4005	0.0446	0.0661	3197.2021	3197.5989	3196.7305	3206.7554
591	3197.3318	0.0490	0.0726	3197.1139	3197.5497	3196.4463	3202.4230
652	3197.2522	0.0291	0.0431	3197.1227	3197.3816	3196.3460	3225.0750
1010	3197.2709	0.0391	0.0580	3197.0970	3197.4448	3196.4710	3197.7520
1094	3197.3394	0.0387	0.0574	3197.1673	3197.5115	3196.8254	3198.7146

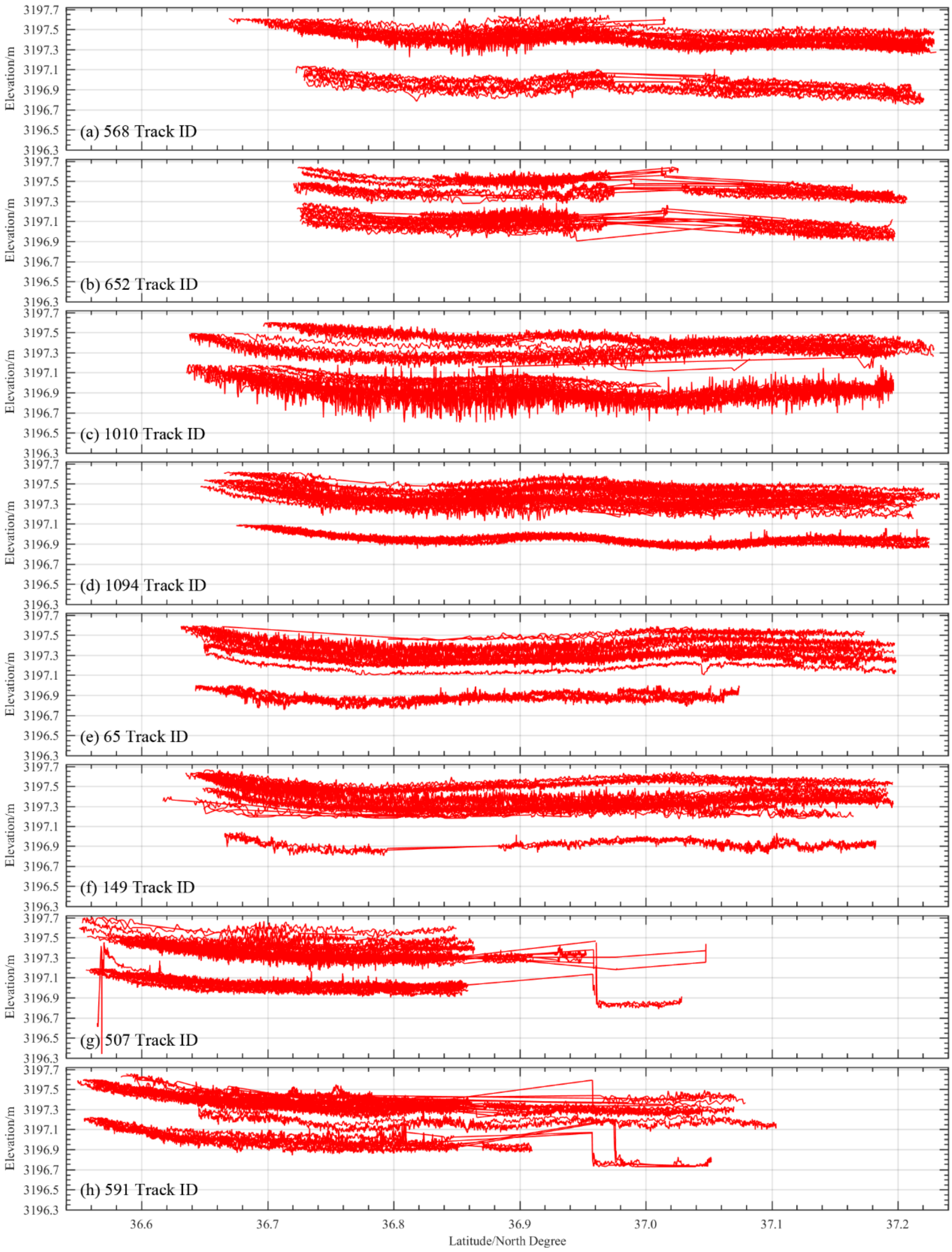

Figure 9. The elevation variation along the latitude in each track of ICESat-2, using the MAD outlier method.

4.2.2. Validation of ICESat-2

We validated the accuracy of the water level data of ICESat-2, which was similar to the ICESat validation. We used the same in-situ water level as that derived from the Xiashe Hydrological Station data. Table A4 presents the matched validation results for ICESat-2 using the Xiashe Hydrological Station data. The first column is the date, the second column is the water level derived from ICESat-2, the third column is the in-situ water level derived from the hydrological station, and the fourth column is the bias of water level (ICESat-2–in-situ). We obtained a total of 13 validation points. The maximum absolute bias value was 0.1350 m, which was recorded on 10 May 2019. Figure 10a shows the scatter diagram of the validation results of the ICESat-2, using the in situ water level. The R was 0.6917, the RMSE was 0.0531 m, the MAE was 0.0647 m, and the ME was 0.0563 m. Only one point was below the 1:1 line, one point was on the 1:1 line, and the other 11 points were above the 1:1 line. The water level figure derived from ICESat-2 was higher than that of the in-situ water level. Figure 10b shows the scatter diagram of the validation results of the ICESat-2 and ICESat using the in-situ water level. Overall, the R increased to 0.9931, the RMSE dropped to 0.1309 m, the MAE was 0.1035 m, and the ME was 0.0260 m. These results showed that the accuracy of ICESat-2 was better than that of ICESat. In addition, ICESat-2 and ICESat could simultaneously observe the changes in regional and global water levels for long periods.

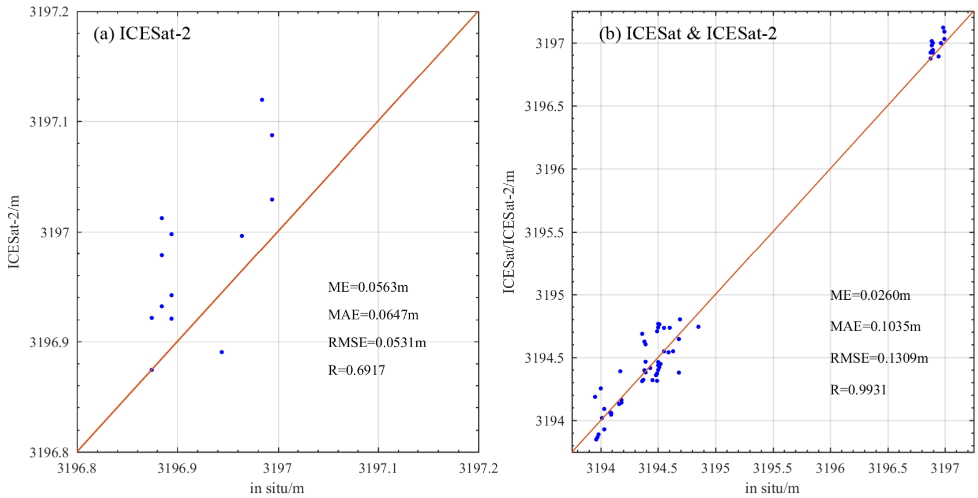

Figure 10. The validation results of the ICESat/ICESat-2 using the in situ water level.

4.3. Water-Level Change in 2003–2020

For the laser altimetry tests, ICESat-2 provided unprecedented accuracy (RMSE = 0.0531 m), followed by ICESat (RMSE = 0.1449 m). We obtained 48 records from 2003 to 2009 (6 years) for ICESat, and the annual data record was 7.3. We obtained 44 records from 2018 to 2020 (2 years) for ICESat-2, and the annual data record was 22. The number of data records was greater than ICESat. Therefore, laser altimetry had a greater capability of monitoring changes in the water level. The in-situ water level (ground data) from the hydrological station is plotted in Figure 11. Furthermore, the uncertainties of ICESat and ICESat-2 were plotted in two parts for mapping and expression. The remote-sensing water level was in good agreement with the in-situ water level. The results showed that the minimum value was 3193.8706 m, recorded on 18 March 2004, and the maximum value was 3197.5290 m, recorded on 5 July 2020. The water level rise was 3.6584 m from 2004 to 2020, although no data were available for ICESat and ICESat-2 for 2010–2018. The rising rate was 0.2287 m/a. The water level fluctuated throughout the year. Generally, the water levels were the lowest in May and the highest in October. The water levels are higher in March because the surface water ice expands under cold conditions. From 2003 to 2009, the maximum value was 3194.7743 m, recorded on 27 February 2008. The water level rise was 0.9037 m from 2004 to 2009 and the rising rate was 0.1807 m/a. The water level rise was 2.2850 m from 2009 to

2018, with no data, and the rising rate was 0.2539 m/a. From 2018 to 2020, the minimum value was 3196.8743 m, recorded on 1 January 2019. The water level rise was 0.5002 m from 2018 to 2020, and the rising rate was 0.2501 m/a.

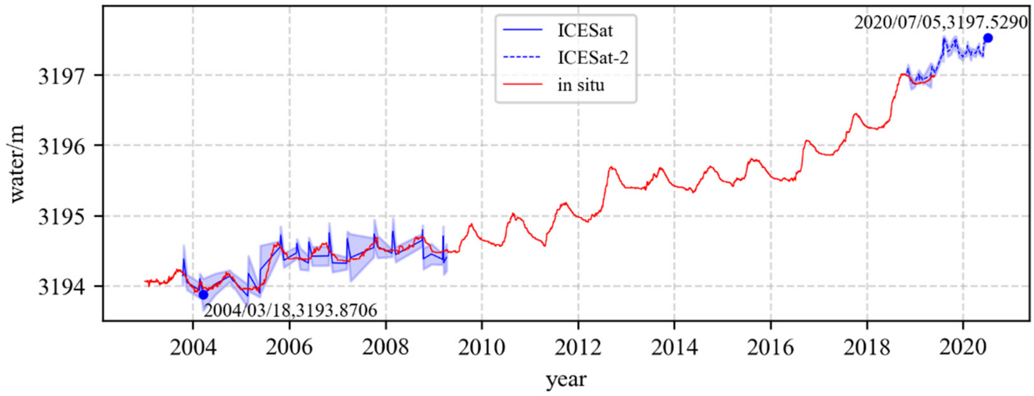

Figure 11. The change and uncertainties in water level derived from ICESat and ICESat-2 with the in situ hydrological station data for 2003–2020.

5. Discussion

Many studies have demonstrated the rapid expansion of an inundated area, an increase in water level, and substantial volume accumulations in the Tibetan lakes [9,79,80]. Qinghai Lake has been in a period of rapid growth since the early 21st century; the water level has increased gradually due to the increased warming-induced meltwater, the possible water sources for this were precipitation and meltwater run-off. The turning point was in 2004; the water level tended to rise sharply by nearly 3.0 m from 2004 to 2018, which was similar to the results obtained in the current study (3.0037 m from 2004 to 2018). The water level was 3194.1426 m on 14 October 2003; the water level rise was by 0.6317 m from 2003 to 2009, which was similar to the previous study [14,18,45,81,82]. The figures are in agreement with the increase and rate of increase of the water level from 2003 to 2020, but the water levels derived from ICESat were estimated by subtracting 0.70 m from the orthometric height, and the water storage change was calculated using the water surface area in the TP [83]. Furthermore, the global lake and reservoir water level changes were monitored for 22,008 lakes and reservoirs with a size greater than 1 km^2, within which the large-scale rising water levels in the TP and the Mississippi River basin in the northern hemisphere were detected [84]

Different satellite platforms used different reference ellipsoids and geoids. ICESat/GLAS used the TOPEX/Poseidon reference ellipsoid and the EGM96 geoid. ICESat-2 used the WGS84 reference ellipsoid and the EGM2008 geoid. Xiashe Hydrological Station used the CGCS2000 reference ellipsoid and the 1985 national elevation benchmarks. There may have been errors in the reference ellipsoid and geoid transfer of ICESat and in the reference ellipsoid and datum transfer of the hydrological station. The equations of transfer may also have been slightly different; therefore, the parameters and the reference ellipsoid and geoid transfer equations in different platforms need further calculation and improvement.

The annual water mask derived from the MODIS was used to mask the water body boundary. The spatial resolution was 250 m and the temporal resolution was one year. Meanwhile, the elevation of some of the lake footprints may not represent the water level of a real lake. Some internal or external water-body pixels may be contained within Qinghai Lake, and these may bring some omission and commission errors. The method used for outlier removal was the MAD outlier method. The outliers were determined outside an interval of the mean plus/minus three standard deviations. The distribution of the water level was heterogeneous, due to the vast extent of Qinghai Lake. The water level along the track is constantly changing as a result of wind interactions. The water level of a large lake is mainly affected by two factors: (1) the surface waves on the surface of the lake, especially the significant wave height; and (2) the still water level on the surface of the lake (still water level can be defined as the average water surface elevation at any instant, excluding local variations due to waves and wave set-up but including the effects of tides, storm surges, and long-term seiches) [85,86]. ICESat only measured the land and water body elevations. ICESat-2 could provide additional measurements of significant wave heights. Therefore, ICESat-2 has the potential to measure the surface wave height of the lake. The water level along the track needs further study and calculations. The lake surface measurements of ICESat showed an absolute accuracy of better than 10 cm in ice-free periods [18], which is similar to the results of this study (MAE = 0.1144 m). The change in water level was retrieved accurately (± 14.1 cm) from ICESat-2 for 3712 global reservoirs (surface areas: 1–10,000 km^2) and the results were better than the global reservoir evaluation results [87].

The water level of the lake on the corresponding date of the ground track was obtained; the median value of each ground track for ICESat was the water level, but it was special for ICESat-2, which had six beams, including six sub-ground tracks. The differences were slightly larger, and the current approach was to calculate the median of the six beams as the water level. The detailed six sub-ground tracks (three pairs) are shown in Figure 12. Figure 12a shows the six sub-ground tracks, and Figure 12b shows the water level along the six sub-ground tracks. There was a noticeable difference between the three pairs, with a weak difference within each pair; the beam spacing is 90 m within pairs and 3.3 km between pairs. The difference between the six beams in the water level also made it possible to detect the higher spatial resolution in the surface water waves.

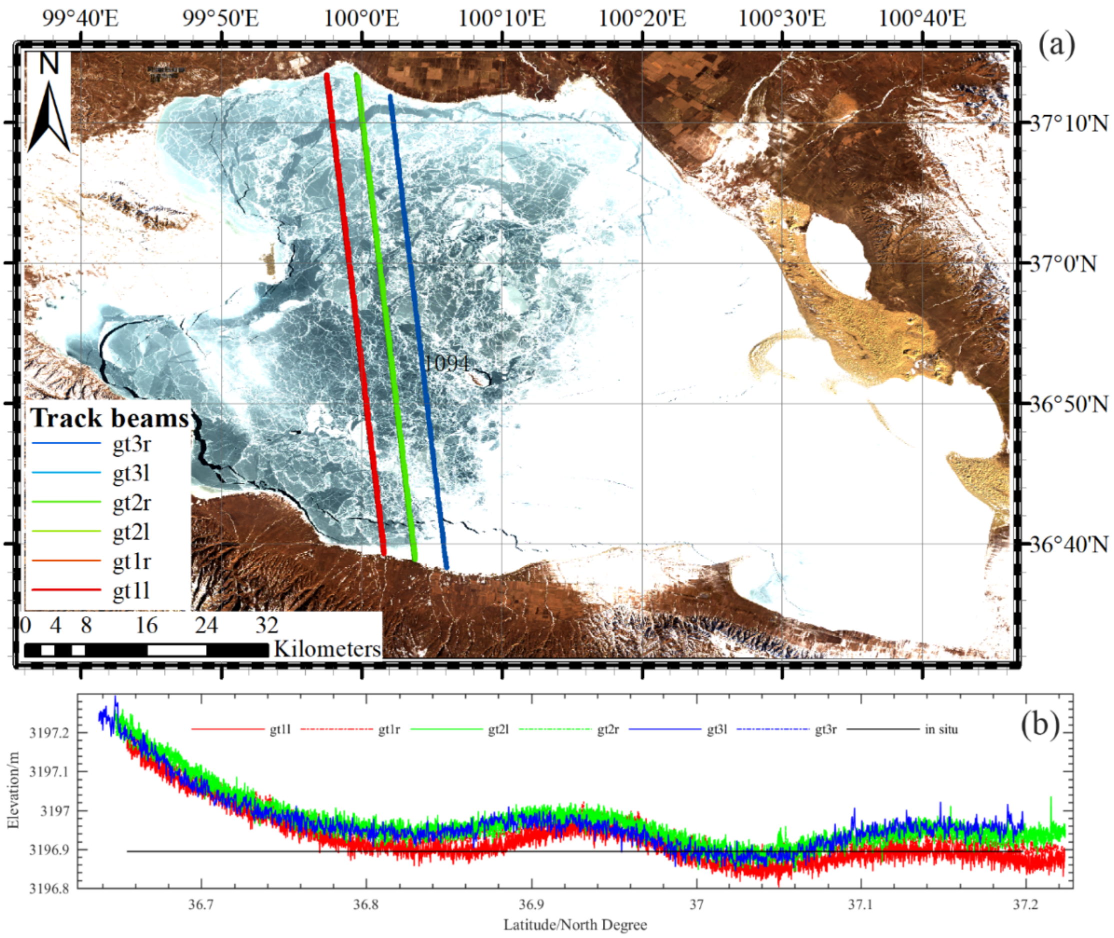

Figure 12. The 1094 Track ID on 10 March 2019 for Qinghai Lake (Landsat 8 OLI 11 January 2019) and the surface water height in gt1l, gt1r, gt2l, gt2r, gt3l, and gt3r on 3 October 2019 (**a**) showed the six sub-ground tracks; (**b**) showed the water 521 level along the six sub-ground tracks).

The laser altimeter offers greater accuracy than a radar altimeter, but only two satellites (ICESat and ICESat-2) can access it. The radar altimeter could be used as a long time-series supplement to monitor water levels in subsequent research, including the Topex/Poseidon, ERS-2, GFO, Jason-1/2/3, Envisat, Cryosat-2, Saral/Altika, and Sentinel 3A/3B/6. Meanwhile, the Gravity Recovery and Climate Experiment (GRACE) and GRACE-Follow-On (GRACE-FO) missions have the ability to calculate water storage changes for large lakes and reservoirs and the water surface area could be monitored by the optical satellite; therefore, the water level of lakes and reservoirs could be derived via inversion. The coarse temporal resolution of the water level also could be reconstructed for the daily water level via deep learning, for which the typical approach used is long short-term memory (LSTM). The next step of this research would focus on the fusion of multiple altimeters and the reconstruction of water level by deep learning; meanwhile, the higher spatial and temporal resolution lake area was combined to calculate the changes in lake water volume.

6. Conclusions

This research focused on the transformation of and changes in the water level of Qinghai Lake, as derived from ICESat and ICESat-2 laser altimetry for 2003–2020, and the ground truth water level derived from the Xiashe Hydrological Station data for 2003–2019. The water level derived from ICESat and ICESat-2 land elevations was preprocessed in each track. The MAD method offers better robustness regarding the satellite ground track data than the other error estimation methods; we were able to extract and remove the outliers of ICESat and ICESat-2 using the MAD outlier removal method. For ICESat, the MAD values ranged from 0.0525 to 0.2470 m, and σ ranged from 0.0778 to 0.3662 m; for ICESat-2, the MAD values ranged from 0.0291 to 0.0490 m, and σ ranged from 0.0431 to 0.0726 m. Both values were less than those of ICESat, and the water level measurement performance was superior to that of ICESat. The WGS84 reference ellipsoid and the EGM2008 geoid were the benchmarks, while the transfer equations were used to convert the water level to the EGM2008 geoid and WGS84 reference ellipsoid. The water levels derived from the Xiashe Hydrological Station and ICESat were transformed to meet this benchmark. The water level of ICESat and ICESat-2 was validated, using the water level derived from the Xiashe Hydrological Station. The validation results showed that the R was 0.8419, the RMSE was 0.1449 m, and the MAE was 0.1144 m for ICESat, while the R was 0.6917, the RMSE was 0.0531 m, and the MAE was 0.0647 m for ICESat-2; high-precision measurement ensured the better observation of water level changes in the lakes. In addition, the validation results of the two combined laser altimeters showed that the R was 0.9931, the RMSE was 0.1309 m, and the MAE was 0.1035 m; the water level of the lake could also be observed with high precision. The change in water level was analyzed for 2003–2020, and the result found that the water level rise was 0.9037 m from 2004 to 2009, and the rising rate was 0.1807 m/a; the water level rise was 0.5002 m from 2018 to 2020, and the rising rate was 0.2501 m/a; the water level rise was 2.2850 m from 2009 to 2018, and the rising rate was 0.2539 m/a. The water level rise was 3.6584 m from 2004 to 2020. The rising rate was 0.2287 m/a.

In conclusion, the water level measurement of the laser altimeters (ICESat and ICESat-2) maintained great accuracy for each ground track. This study, however, did have some limitations, such as coarse temporal resolution and differences in the geographic positions of tracks. Further research will focus on the reconstruction of the daily water level of other remote mid-sized and small lakes. The six beams of ICESat-2 will be crucial to achieving greater research potential.

Author Contributions: Conceptualization, W.H. and C.H.; methodology, W.H.; software, W.H.; validation, W.H.; formal analysis, W.H. and J.H.; investigation, W.H.; resources, C.H. and W.W.; data curation, W.H.; writing—original draft preparation, W.H.; writing—review and editing, C.H., J.G., J.H., W.W. and Y.Z.; visualization, W.H.; supervision, C.H. and W.W.; project administration, C.H., W.H. and J.H.; funding acquisition, C.H., J.G., W.H. and J.H. All authors have read and agreed to the published version of the manuscript.

Funding: This research was funded by the Strategic Priority Research Program of the Chinese Academy of Sciences "CAS Earth Big Data Science Project" (Project No. XDA19040504), the National Natural Science Foundation of China (Project No. 42130113), and the Gansu Science and Technology Program (Project No. 22JR5RA090) under Grants.

Data Availability Statement: The ICESat data is available on the website: https://nsidc.org/data/GLA14/versions/34 (5 December 2022); The ICESat-2 data is available on the website: https://openaltimetry.org/data/icesat2/ (5 December 2022); The water-level dataset was provided by the Data Center for Eco-Environment Protection in the Qinghai Lake Basin (http://qhh.qhemdc.cn/ (5 December 2022)).

Acknowledgments: We are grateful for the use of the Google Earth Engine, NASADEM, and MOD44W V6 data in this study.

Conflicts of Interest: The authors declare no conflict of interest.

Appendix A

Table A1. The parameters of the MAD outlier method for the corresponding dates of ICESat.

Date	Track	M	MAD	σ	σ	σ	Min	Max
14/10/2003	1239	3149.3610	0.1040	0.1542	3148.8984	3149.8236	3148.5610	3153.1570
18/10/2003	1306	3149.4170	0.0840	0.1245	3149.0434	3149.7906	3148.8500	3151.4060
22/10/2003	4	3150.2190	0.0505	0.0749	3149.9944	3150.4436	3148.4040	3150.4320
16/11/2003	376	3149.4080	0.0820	0.1216	3149.0433	3149.7727	3149.2410	3152.5610
19/02/2004	1306	3149.1740	0.0660	0.0979	3148.8804	3149.4676	3148.8750	3152.0230
22/02/2004	4	3149.9235	0.0375	0.0556	3149.7567	3150.0903	3149.8150	3150.1460
18/03/2004	376	3149.2780	0.1080	0.1601	3148.7976	3149.7584	3148.7590	3152.5040
20/05/2004	1306	3148.2990	0.4960	0.7354	3146.0929	3150.5051	3147.7000	3154.0590
17/06/2004	376	3149.3685	0.0865	0.1282	3148.9838	3149.7532	3148.0690	3152.5780
06/10/2004	1306	3149.4110	0.0720	0.1067	3149.0908	3149.7312	3149.0970	3156.9160
03/11/2004	376	3149.4270	0.0870	0.1290	3149.0400	3149.8140	3148.2100	3152.2790
08/11/2004	443	3149.4660	0.0525	0.0778	3149.2325	3149.6995	3148.1810	3152.5440
20/02/2005	1306	3149.0840	0.2110	0.3128	3148.1455	3150.0225	3148.7600	3152.6270
24/02/2005	4	3150.0160	0.0525	0.0778	3149.7825	3150.2495	3149.1380	3154.2530
22/05/2005	1306	3149.1085	0.0565	0.0838	3148.8572	3149.3598	3148.9580	3149.4390
26/05/2005	4	3150.0560	0.0670	0.0993	3149.7580	3150.3540	3147.7580	3150.1950
23/10/2005	1306	3149.7940	0.0730	0.1082	3149.4693	3150.1187	3149.6490	3151.0830
27/10/2005	4	3150.5720	0.0380	0.0563	3150.4030	3150.7410	3150.3310	3150.7940
21/11/2005	376	3149.7135	0.0885	0.1312	3149.3199	3150.1071	3148.4730	3152.3130
24/02/2006	1306	3149.7195	0.1040	0.1542	3149.2569	3150.1821	3149.4930	3151.7300
27/02/2006	4	3150.4430	0.0380	0.0563	3150.2740	3150.6120	3150.3620	3150.6850
24/03/2006	376	3149.7350	0.0810	0.1201	3149.3747	3150.0953	3148.0560	3152.6870
26/05/2006	1306	3149.5785	0.0980	0.1453	3149.1426	3150.0144	3149.3570	3153.2280
29/05/2006	4	3150.4790	0.0510	0.0756	3150.2522	3150.7058	3150.3210	3150.7280
23/06/2006	376	3149.7880	0.0980	0.1453	3149.3521	3150.2239	3149.1770	3152.6930
27/10/2006	1306	3149.6705	0.0735	0.1090	3149.3436	3149.9974	3149.2910	3150.4330
30/10/2006	4	3150.6190	0.0770	0.1142	3150.2765	3150.9615	3150.3350	3151.9620
24/11/2006	376	3149.6630	0.0750	0.1112	3149.3294	3149.9966	3149.3330	3151.1560
13/03/2007	1306	3149.6620	0.0360	0.0534	3149.5019	3149.8221	3149.5200	3150.0200
17/03/2007	4	3150.5620	0.0670	0.0993	3150.2640	3150.8600	3150.3220	3158.2440
11/04/2007	376	3149.8600	0.3165	0.4692	3148.4523	3151.2677	3149.3190	3153.1860
04/10/2007	1306	3149.8580	0.1255	0.1861	3149.2998	3150.4162	3149.4610	4781.5790
08/10/2007	4	3150.6580	0.0600	0.0890	3150.3911	3150.9249	3150.3280	3151.2490
02/11/2007	376	3149.9015	0.0850	0.1260	3149.5234	3150.2796	3148.5240	3152.4240
19/02/2008	1306	3149.8020	0.1045	0.1549	3149.3372	3150.2668	3149.5480	3173.1230
22/02/2008	4	3150.5820	0.0595	0.0882	3150.3174	3150.8466	3150.4190	3150.8590
27/02/2008	71	3150.5230	0.1050	0.1557	3150.0560	3150.9900	3150.3240	3153.7340
18/03/2008	376	3149.7730	0.0520	0.0771	3149.5417	3150.0043	3149.4270	3151.3500

Table A1. *Cont.*

Date	Track	M	MAD	σ	σ	σ	Min	Max
06/10/2008	1306	3149.9030	0.0930	0.1379	3149.4894	3150.3166	3149.6300	3152.2210
09/10/2008	4	3150.6310	0.0480	0.0712	3150.4175	3150.8445	3150.4000	3150.8650
14/10/2008	71	3150.1200	0.1095	0.1623	3149.6330	3150.6070	3149.8110	3153.4950
14/12/2008	376	3149.8105	0.0865	0.1282	3149.4258	3150.1952	3149.3640	3155.9920
10/03/2009	1306	3149.6260	0.0510	0.0756	3149.3992	3149.8528	3149.4120	3149.7290
14/03/2009	4	3150.5730	0.0670	0.0993	3150.2750	3150.8710	3150.3550	3154.2580
18/03/2009	71	3150.0755	0.1085	0.1609	3149.5929	3150.5581	3149.7200	3153.3600
08/04/2009	376	3149.8580	0.1830	0.2713	3149.0441	3150.6719	3149.6370	3152.5690
02/10/2009	1306	3150.0040	0.0940	0.1394	3149.5859	3150.4221	3149.6200	3152.6030

Table A2. The validation for ICESat, using the in situ station data (the underlined point is excluded from further assessment).

Date	ICESat/m	In Situ/m	Bias/m	Date	ICESat/m	In Situ/m	Bias/m
14/10/2003	3194.1426	3194.1822	−0.0396	23/06/2006	3194.4160	3194.4322	−0.0162
18/10/2003	3194.1629	3194.1822	−0.0193	27/10/2006	3194.4231	3194.5122	−0.0891
22/10/2003	3194.3903	3194.1722	0.2181	30/10/2006	3194.7624	3194.5122	0.2502
16/11/2003	3194.0468	3194.0922	−0.0454	24/11/2006	3194.3200	3194.4522	−0.1322
19/02/2004	3193.9296	3194.0322	−0.1026	13/03/2007	3194.3122	3194.3622	−0.0500
22/02/2004	3194.0914	3194.0322	0.0592	17/03/2007	3194.6874	3194.3622	0.3252
18/03/2004	3193.8656	3193.9722	−0.1066	11/04/2007	3194.3986	3194.3822	0.0164
20/05/2004	3193.0000	3193.9622	−0.9622	04/10/2007	3194.5407	3194.5922	−0.0515
17/06/2004	3194.0195	3194.0122	0.0073	08/10/2007	3194.7357	3194.6022	0.1335
06/10/2004	3194.1307	3194.1622	−0.0315	02/11/2007	3194.5490	3194.6322	−0.0832
03/11/2004	3194.0602	3194.0922	−0.0320	19/02/2008	3194.4633	3194.5022	−0.0389
08/11/2004	3194.0647	3194.0822	−0.0175	22/02/2008	3194.7377	3194.5022	0.2355
20/02/2005	3193.8500	3193.9622	−0.1122	27/02/2008	3194.7666	3194.5022	0.2644
24/02/2005	3194.1872	3193.9522	0.2350	18/03/2008	3194.4374	3194.5022	−0.0648
22/05/2005	3193.8900	3193.9822	−0.0922	06/10/2008	3194.6458	3194.6822	−0.0364
26/05/2005	3194.2541	3194.0022	0.2519	09/10/2008	3194.8020	3194.6922	0.1098
23/10/2005	3194.5480	3194.5522	−0.0042	14/10/2008	3194.3799	3194.6822	−0.3023
27/10/2005	3194.7340	3194.5522	0.1818	14/12/2008	3194.4477	3194.5222	−0.0745
21/11/2005	3194.3592	3194.4822	−0.1230	10/03/2009	3194.3732	3194.4922	−0.1190
24/02/2006	3194.4660	3194.3922	0.0738	14/03/2009	3194.7073	3194.4922	0.2151
27/02/2006	3194.6040	3194.3922	0.2118	18/03/2009	3194.3146	3194.4922	−0.1776
24/03/2006	3194.3813	3194.3922	−0.0109	08/04/2009	3194.4016	3194.5022	−0.1006
26/05/2006	3194.3225	3194.3722	−0.0497	02/10/2009	3194.7432	3194.8522	−0.1090
29/05/2006	3194.6258	3194.3822	0.2436				

Table A3. The parameters of the MAD outlier method for the corresponding dates of ICESat-2.

Date	Track	M	MAD	σ	σ	σ	Min	Min
31/10/2018	507	3197.0319	0.0269	0.0400	3196.9120	3197.1517	3195.3083	3197.3267
10/11/2018	652	3197.0874	0.0447	0.0663	3196.8886	3197.2862	3196.3560	3199.8335
03/12/2018	1010	3196.8918	0.0653	0.0968	3196.6014	3197.1822	3196.4710	3197.5435
01/01/2019	65	3196.8745	0.0281	0.0417	3196.7495	3196.9995	3196.7197	3199.0810
07/01/2019	149	3196.9214	0.0283	0.0420	3196.7955	3197.0473	3196.7236	3197.8706
30/01/2019	507	3197.0142	0.0395	0.0586	3196.8385	3197.1899	3196.9004	3197.4950
03/02/2019	568	3196.9324	0.0449	0.0666	3196.7327	3197.1321	3196.7305	3197.2004
05/02/2019	591	3196.9710	0.0556	0.0824	3196.7239	3197.2181	3196.4463	3198.5261
09/02/2019	652	3196.9988	0.0303	0.0449	3196.8640	3197.1336	3196.8960	3199.3718
04/03/2019	1010	3196.9268	0.0380	0.0563	3196.7578	3197.0958	3196.8232	3197.4172

Table A3. *Cont.*

Date	Track	M	MAD	σ	σ	σ	Min	Min
10/03/2019	1094	3196.9460	0.0320	0.0474	3196.8037	3197.0883	3196.8254	3197.7234
01/05/2019	507	3196.9957	0.1543	0.2288	3196.3092	3197.6822	3195.9036	3199.5193
10/05/2019	652	3197.1220	0.0255	0.0378	3197.0086	3197.2354	3196.3460	3199.8610
03/06/2019	1010	3197.0398	0.0298	0.0442	3196.9073	3197.1723	3196.9248	3197.3562
31/07/2019	507	3197.3162	0.0354	0.0525	3197.1587	3197.4737	3196.8142	3199.3313
04/08/2019	568	3197.5017	0.0335	0.0497	3197.3527	3197.6507	3197.1624	3206.7554
05/08/2019	591	3197.2856	0.0551	0.0817	3197.0405	3197.5307	3197.0452	3201.0264
09/08/2019	652	3197.5242	0.0279	0.0414	3197.4001	3197.6483	3197.3916	3225.0750
02/09/2019	1010	3197.4275	0.0391	0.0580	3197.2536	3197.6014	3197.2568	3197.7520
07/09/2019	1094	3197.3416	0.0449	0.0666	3197.1419	3197.5413	3197.0996	3197.6536
01/10/2019	65	3197.3672	0.0518	0.0768	3197.1368	3197.5976	3197.1467	3197.6533
06/10/2019	149	3197.4019	0.0529	0.0784	3197.1666	3197.6372	3197.1616	3198.9220
30/10/2019	507	3197.4937	0.0477	0.0707	3197.2815	3197.7059	3197.3208	3200.8225
03/11/2019	568	3197.4080	0.0456	0.0676	3197.2052	3197.6108	3197.1970	3197.7524
04/11/2019	591	3197.4382	0.0490	0.0726	3197.2203	3197.6561	3197.2910	3197.7036
08/11/2019	652	3197.5032	0.0315	0.0467	3197.3631	3197.6433	3196.7175	3200.1177
02/12/2019	1010	3197.3088	0.0408	0.0605	3197.1273	3197.4903	3197.1333	3197.6780
07/12/2019	1094	3197.3200	0.0460	0.0682	3197.1154	3197.5246	3197.0970	3197.6494
30/12/2019	65	3197.2590	0.0356	0.0528	3197.1007	3197.4173	3197.0645	3197.8610
05/01/2020	149	3197.2927	0.0254	0.0377	3197.1797	3197.4057	3197.0063	3197.4465
28/01/2020	507	3197.3135	0.0320	0.0474	3197.1712	3197.4558	3196.7650	3199.1064
03/02/2020	591	3197.4170	0.0410	0.0608	3197.2346	3197.5994	3196.8748	3202.4230
07/02/2020	652	3197.3823	0.0249	0.0369	3197.2715	3197.4931	3197.2146	3197.5930
01/03/2020	1010	3197.2832	0.0535	0.0793	3197.0452	3197.5212	3197.0305	3197.3716
07/03/2020	1094	3197.3394	0.0314	0.0466	3197.1997	3197.4791	3197.1887	3198.7146
05/04/2020	149	3197.3088	0.0396	0.0587	3197.1327	3197.4849	3197.1948	3197.5405
28/04/2020	507	3197.4090	0.0240	0.0356	3197.3023	3197.5157	3197.3054	3197.6902
02/05/2020	568	3197.3930	0.0443	0.0657	3197.1960	3197.5900	3197.2550	3197.6220
04/05/2020	591	3197.3318	0.0272	0.0403	3197.2108	3197.4528	3197.2188	3197.6396
31/05/2020	1010	3197.2709	0.0120	0.0179	3197.2173	3197.3245	3197.2400	3197.4082
06/06/2020	1094	3197.4440	0.0387	0.0574	3197.2719	3197.6161	3197.3137	3197.8300
29/06/2020	65	3197.5205	0.0164	0.0243	3197.4476	3197.5934	3197.3547	3200.3542
05/07/2020	149	3197.5290	0.0307	0.0455	3197.3925	3197.6655	3197.3720	3197.6995

Table A4. The validation for ICESat-2, using the in situ station.

Date	ICESat-2/m	In Situ/m	Bias/m	Date	ICESat-2/m	In Situ/m	Bias/m
31/10/2018	3197.0288	3196.9944	0.0344	05/02/2019	3196.978	3196.8844	0.0936
10/11/2018	3197.0872	3196.9944	0.0928	09/02/2019	3196.9976	3196.8944	0.1032
03/12/2018	3196.8901	3196.9444	−0.0543	04/03/2019	3196.9204	3196.8944	0.0260
01/01/2019	3196.8743	3196.8744	−0.0001	10/03/2019	3196.942	3196.8944	0.0476
07/01/2019	3196.9214	3196.8744	0.0470	01/05/2019	3196.9962	3196.9644	0.0318
30/01/2019	3197.0122	3196.8844	0.1278	10/05/2019	3197.1194	3196.9844	0.1350
03/02/2019	3196.932	3196.8844	0.0476				

References

1. Gleick, P.H. Global freshwater resources: Soft-path solutions for the 21st century. *Science* **2003**, *302*, 1524–1528. [CrossRef]
2. Tranvik, L.J.; Downing, J.A.; Cotner, J.B.; Loiselle, S.A.; Striegl, R.G.; Ballatore, T.J.; Dillon, P.; Finlay, K.; Fortino, K.; Knoll, L.B. Lakes and reservoirs as regulators of carbon cycling and climate. *Limnol. Oceanogr.* **2009**, *54*, 2298–2314. [CrossRef]
3. Verpoorter, C.; Kutser, T.; Seekell, D.A.; Tranvik, L.J. A global inventory of lakes based on high-resolution satellite imagery. *Geophys. Res. Lett.* **2014**, *41*, 6396–6402. [CrossRef]
4. Williamson, C.E.; Saros, J.E.; Vincent, W.F.; Smol, J.P. Lakes and reservoirs as sentinels, integrators, and regulators of climate change. *Limnol. Oceanogr.* **2009**, *54*, 2273–2282. [CrossRef]
5. Pekel, J.-F.; Cottam, A.; Gorelick, N.; Belward, A.S. High-resolution mapping of global surface water and its long-term changes. *Nature* **2016**, *540*, 418–422. [CrossRef]

6. Palmer, S.C.J.; Kutser, T.; Hunter, P.D. Remote sensing of inland waters: Challenges, progress and future directions. *Remote Sens. Environ.* **2015**, *157*, 1–8. [CrossRef]
7. Li, P.; Li, H.; Chen, F.; Cai, X. Monitoring Long-Term Lake Level Variations in Middle and Lower Yangtze Basin over 2002–2017 through Integration of Multiple Satellite Altimetry Datasets. *Remote Sens.* **2020**, *12*, 1448. [CrossRef]
8. Ma, Y.; Xu, N.; Zhang, W.; Wang, X.H.; Sun, J.; Feng, X.; Sun, Y. Increasing Water Levels of Global Lakes between 2003 and 2009. *IEEE Geosci. Remote Sens. Lett.* **2020**, *17*, 187–191. [CrossRef]
9. Mohamed, A. Gravity applications in estimating the mass variations in the Middle East: A case study from Iran. *Arab. J. Geosci.* **2020**, *13*, 364. [CrossRef]
10. Al-Abadi, A.M.; Ghalib, H.B.; Al-Mohammdawi, J.A. Delineation of Groundwater Recharge Zones in Ali Al-Gharbi District, Southern Iraq Using Multi-criteria Decision-making Model and GIS. *J. Geovisualization Spat. Anal.* **2020**, *4*, 9. [CrossRef]
11. Zhang, G.; Chen, W.; Xie, H. Tibetan Plateau's lake level and volume changes from NASA's ICESat/ICESat-2 and Landsat Missions. *Geophys. Res. Lett.* **2019**, *46*, 13107–13118. [CrossRef]
12. Lu, C.; Yu, G.; Xie, G. Tibetan plateau serves as a water tower. In Proceedings of the IGARSS 2005—IEEE International Geoscience and Remote Sensing Symposium, Seoul, Republic of Korea, 29 July 2005; pp. 3120–3123.
13. Immerzeel, W.W.; Van Beek, L.P.; Bierkens, M.F. Climate change will affect the Asian water towers. *Science* **2010**, *328*, 1382–1385. [CrossRef] [PubMed]
14. Wan, W.; Xiao, P.; Feng, X.; Li, H.; Ma, R.; Duan, H.; Zhao, L. Monitoring lake changes of Qinghai-Tibetan Plateau over the past 30 years using satellite remote sensing data. *Chin. Sci. Bull.* **2014**, *59*, 1021–1035. [CrossRef]
15. Zhou, J.; Wang, L.; Zhang, Y.; Guo, Y.; Li, X.; Liu, W. Exploring the water storage changes in the largest lake (Selin Co) over the Tibetan Plateau during 2003–2012 from a basin-wide hydrological modeling. *Water Resour. Res.* **2015**, *51*, 8060–8086. [CrossRef]
16. Shen, Y.; Chen, H.; Xu, C. Remote Sensing Monitoring Study for the Tendency of Qinghai Lake's Water Area in Last 41 Years. *J. Water Resour. Res.* **2013**, *2*, 309–315.
17. Fang, J.; Li, G.; Rubinato, M.; Ma, G.; Zhou, J.; Jia, G.; Yu, X.; Wang, H. Analysis of Long-Term Water Level Variations in Qinghai Lake in China. *Water* **2019**, *11*, 2136. [CrossRef]
18. Zhang, G.; Xie, H.; Kang, S.; Yi, D.; Ackley, S.F. Monitoring lake level changes on the Tibetan Plateau using ICESat altimetry data (2003–2009). *Remote Sens. Environ.* **2011**, *115*, 1733–1742. [CrossRef]
19. Jiang, L.; Nielsen, K.; Andersen, O.B.; Bauer-Gottwein, P. Monitoring recent lake level variations on the Tibetan Plateau using CryoSat-2 SARIn mode data. *J. Hydrol.* **2017**, *544*, 109–124. [CrossRef]
20. Song, C.; Huang, B.; Richards, K.; Ke, L.; Hien Phan, V. Accelerated lake expansion on the Tibetan Plateau in the 2000s: Induced by glacial melting or other processes? *Water Resour. Res.* **2014**, *50*, 3170–3186. [CrossRef]
21. Wang, X.; Gong, P.; Zhao, Y.; Xu, Y.; Cheng, X.; Niu, Z.; Luo, Z.; Huang, H.; Sun, F.; Li, X. Water-level changes in China's large lakes determined from ICESat/GLAS data. *Remote Sens. Environ.* **2013**, *132*, 131–144. [CrossRef]
22. Crétaux, J.-F.; Birkett, C. Lake studies from satellite radar altimetry. *Comptes Rendus Geosci.* **2006**, *338*, 1098–1112. [CrossRef]
23. Shiklomanov, A.I.; Lammers, R.B.; Vörösmarty, C.J. Widespread decline in hydrological monitoring threatens pan-Arctic research. *Eos Trans. Am. Geophys. Union* **2002**, *83*, 13–17. [CrossRef]
24. Lawford, R.; Strauch, A.; Toll, D.; Fekete, B.; Cripe, D. Earth observations for global water security. *Curr. Opin. Environ. Sustain.* **2013**, *5*, 633–643. [CrossRef]
25. Han, W.; Huang, C.; Duan, H.; Gu, J.; Hou, J. Lake Phenology of Freeze-Thaw Cycles Using Random Forest: A Case Study of Qinghai Lake. *Remote Sens.* **2020**, *12*, 4098. [CrossRef]
26. Peng, Y.; Li, Z.; Xu, C.; Zhang, H.; Han, W. Surface Velocity Analysis of Surge Region of Karayaylak Glacier from 2014 to 2020 in the Pamir Plateau. *Remote Sens.* **2021**, *13*, 774. [CrossRef]
27. Liu, D.; Duan, H.; Loiselle, S.; Hu, C.; Zhang, G.; Li, J.; Yang, H.; Thompson, J.R.; Cao, Z.; Shen, M.; et al. Observations of water transparency in China's lakes from space. *Int. J. Appl. Earth Obs. Geoinf.* **2020**, *92*, 102187. [CrossRef]
28. Nhu, V.-H.; Mohammadi, A.; Shahabi, H.; Shirzadi, A.; Al-Ansari, N.; Ahmad, B.B.; Chen, W.; Khodadadi, M.; Ahmadi, M.; Khosravi, K.; et al. Monitoring and Assessment of Water Level Fluctuations of the Lake Urmia and Its Environmental Consequences Using Multitemporal Landsat 7 ETM+ Images. *Int. J. Environ. Res. Public Health* **2020**, *17*, 4210. [CrossRef]
29. El-Shirbeny, M.A.; Abutaleb, K.A. Monitoring of Water-Level Fluctuation of Lake Nasser Using Altimetry Satellite Data. *Earth Syst. Environ.* **2018**, *2*, 367–375. [CrossRef]
30. Berry, P.A.M.; Garlick, J.D.; Freeman, J.A.; Mathers, E.L. Global inland water monitoring from multi-mission altimetry. *Geophys. Res. Lett.* **2005**, *32*, 1–4. [CrossRef]
31. Birkett, C.M. The contribution of TOPEX/POSEIDON to the global monitoring of climatically sensitive lakes. *J. Geophys. Res. Ocean.* **1995**, *100*, 25179–25204. [CrossRef]
32. Crétaux, J.F.; Abarca-del-Río, R.; Bergé-Nguyen, M.; Arsen, A.; Drolon, V.; Clos, G.; Maisongrande, P. Lake Volume Monitoring from Space. *Surv. Geophys.* **2016**, *37*, 269–305. [CrossRef]
33. Gao, L.; Liao, J.; Shen, G. Monitoring lake-level changes in the Qinghai–Tibetan Plateau using radar altimeter data (2002–2012). *J. Appl. Remote Sens.* **2013**, *7*, 073470. [CrossRef]
34. Kleinherenbrink, M.; Lindenbergh, R.C.; Ditmar, P.G. Monitoring of lake level changes on the Tibetan Plateau and Tian Shan by retracking Cryosat SARIn waveforms. *J. Hydrol.* **2015**, *521*, 119–131. [CrossRef]

35. Liao, J.; Gao, L.; Wang, X. Numerical Simulation and Forecasting of Water Level for Qinghai Lake Using Multi-Altimeter Data Between 2002 and 2012. *IEEE J. Sel. Top. Appl. Earth Obs. Remote Sens.* **2014**, *7*, 609–622. [CrossRef]
36. Song, C.; Huang, B.; Ke, L. Heterogeneous change patterns of water level for inland lakes in High Mountain Asia derived from multi-mission satellite altimetry. *Hydrol. Process.* **2015**, *29*, 2769–2781. [CrossRef]
37. Song, C.; Huang, B.; Ke, L.; Richards, K.S. Seasonal and abrupt changes in the water level of closed lakes on the Tibetan Plateau and implications for climate impacts. *J. Hydrol.* **2014**, *514*, 131–144. [CrossRef]
38. Song, C.; Ye, Q.; Cheng, X. Shifts in water-level variation of Namco in the central Tibetan Plateau from ICESat and CryoSat-2 altimetry and station observations. *Sci. Bull.* **2015**, *60*, 1287–1297. [CrossRef]
39. Song, C.; Ye, Q.; Sheng, Y.; Gong, T. Combined ICESat and CryoSat-2 Altimetry for Accessing Water Level Dynamics of Tibetan Lakes over 2003–2014. *Water* **2015**, *7*, 4685–4700. [CrossRef]
40. Schutz, B.E.; Zwally, H.J.; Shuman, C.A.; Hancock, D.; DiMarzio, J.P. Overview of the ICESat Mission. *Geophys. Res. Lett.* **2005**, *32*, 1–4. [CrossRef]
41. Markus, T.; Neumann, T.; Martino, A.; Abdalati, W.; Brunt, K.; Csatho, B.; Farrell, S.; Fricker, H.; Gardner, A.; Harding, D. The Ice, Cloud, and land Elevation Satellite-2 (ICESat-2): Science requirements, concept, and implementation. *Remote Sens. Environ.* **2017**, *190*, 260–273. [CrossRef]
42. Su, D.; Hu, X.; Wen, L.; Lyu, S.; Gao, X.; Zhao, L.; Li, Z.; Du, J.; Kirillin, G. Numerical study on the response of the largest lake in China to climate change. *Hydrol. Earth Syst. Sci.* **2019**, *23*, 2093–2109. [CrossRef]
43. Guoqing, Z. Dataset of river basins map over the TP (2016). *Natl. Tibet. Plateau Data Cent.* **2019**. [CrossRef]
44. Zhang, G.; Yao, T.; Xie, H.; Kang, S.; Lei, Y. Increased mass over the Tibetan Plateau: From lakes or glaciers? *Geophys. Res. Lett.* **2013**, *40*, 2125–2130. [CrossRef]
45. Yuan, Y.; Li, D.L.; An, D. Response of water level in Qinghai Lake to climate change in the Qinghai-Xizang Plateau. *Plat. Meteorol.* **2012**, *31*, 57–64.
46. Ao, H.; Wu, C.; Xiong, X.; Jing, L.; Huang, X.; Zhang, K.; Liu, J. Water and sediment quality in Qinghai Lake, China: A revisit after half a century. *Environ. Monit. Assess.* **2014**, *186*, 2121–2133. [CrossRef] [PubMed]
47. ChongYi, E.; Zhang, J.; Chen, Z.Y.; Sun, Y.J.; Zhao, Y.J.; Li, P.; Sun, M.P.; Shi, Y.K. High resolution OSL dating of aeolian activity at Qinghai Lake, Northeast Tibetan Plateau. *CATENA* **2019**, *183*, 104180. [CrossRef]
48. Wang, Y.; Jin, Z.; Zhou, L.; Li, F.; Zhang, F.; Chen, L.; Qiu, X.; Qi, R. Stratigraphy and otolith microchemistry of the naked carp *Gymnocypris przewalskii* (Kessler) and their indication for water level of Lake Qinghai during the Ming Dynasty of China. *Sci. China Earth Sci.* **2014**, *57*, 2512–2521. [CrossRef]
49. Han, W.; Huang, C.; Wang, Y.; Gu, J. Study on the Area Variation of Qinghai Lake Based on Long-Term Landsat 5/8 Multi-Band Remote Sensing Imagery. *Adv. Earth Sci.* **2019**, *34*, 346–355. [CrossRef]
50. Wei, H.; Chongyi, E.; Zhang, J.; Sun, Y.; Li, Q.; Hou, G.; Duan, R. Climate change and anthropogenic activities in Qinghai Lake basin over the last 8500 years derived from pollen and charcoal records in an aeolian section. *CATENA* **2020**, *193*, 104616. [CrossRef]
51. Ding, Z.; Lu, R.; Lyu, Z.; Liu, X. Geochemical characteristics of Holocene aeolian deposits east of Qinghai Lake, China, and their paleoclimatic implications. *Sci. Total Environ.* **2019**, *692*, 917–929. [CrossRef]
52. Li, X.-Y.; Xu, H.-Y.; Sun, Y.-L.; Zhang, D.-S.; Yang, Z.-P. Lake-Level Change and Water Balance Analysis at Lake Qinghai, West China during Recent Decades. *Water Resour. Manag.* **2007**, *21*, 1505–1516. [CrossRef]
53. Cai, Y.; Ke, C.-Q.; Duan, Z. Monitoring ice variations in Qinghai Lake from 1979 to 2016 using passive microwave remote sensing data. *Sci. Total Environ.* **2017**, *607*, 120–131. [CrossRef] [PubMed]
54. Yin, Q.J.; Yang, Y.L. Remote sensing monitoring of Lake Qinghai based on EOS/MODIS data. *J. Lake Sci.* **2005**, *17*, 356–360.
55. Che, T.; Li, X.; Jin, R. Monitoring the frozen duration of Qinghai Lake using satellite passive microwave remote sensing low frequency data. *Chin. Sci. Bull.* **2009**, *54*, 787–791. [CrossRef]
56. Phan, V.H.; Lindenbergh, R.; Menenti, M. ICESat derived elevation changes of Tibetan lakes between 2003 and 2009. *Int. J. Appl. Earth Obs. Geoinf.* **2012**, *17*, 12–22. [CrossRef]
57. Duan, Z.; Bastiaanssen, W.; Muala, E. Icesat-derived water level variations of roseires reservoir (Sudan) in the Nile basin. In Proceedings of the 2013 IEEE International Geoscience and Remote Sensing Symposium-IGARSS, Melbourne, Australia, 21–26 July 2013; pp. 2884–2887.
58. Duan, Z.; Bastiaanssen, W. Estimating water volume variations in lakes and reservoirs from four operational satellite altimetry databases and satellite imagery data. *Remote Sens. Environ.* **2013**, *134*, 403–416. [CrossRef]
59. Kwok, R.; Zwally, H.J.; Yi, D. ICESat observations of Arctic sea ice: A first look. *Geophys. Res. Lett.* **2004**, *31*. [CrossRef]
60. Zwally, H.J.; Yi, D.; Kwok, R.; Zhao, Y. ICESat measurements of sea ice freeboard and estimates of sea ice thickness in the Weddell Sea. *J. Geophys. Res. Ocean.* **2008**, *113*, 1–17. [CrossRef]
61. Bhang, K.J.; Schwartz, F.W.; Braun, A. Verification of the vertical error in C-band SRTM DEM using ICESat and Landsat-7, Otter Tail County, MN. *IEEE Trans. Geosci. Remote Sens.* **2006**, *45*, 36–44. [CrossRef]
62. Braun, A.; Cheng, K.-C.; Csatho, B.; Shum, C. ICESat laser altimetry in the Great Lakes. In *Proceedings of the Proceedings of the 60th Annual Meeting of The Institute of Navigation (2004), Dayton, OH, USA, 7–9 June 2004*; pp. 409–416.
63. Swenson, S.; Wahr, J. Monitoring the water balance of Lake Victoria, East Africa, from space. *J. Hydrol.* **2009**, *370*, 163–176. [CrossRef]

64. Urban, T.J.; Schutz, B.E.; Neuenschwander, A.L. A survey of ICESat coastal altimetry applications: Continental coast, open ocean island, and inland river. *Terr. Atmos. Ocean. Sci.* **2008**, *19*, 1–19. [CrossRef]
65. Jasinski, M.; Stoll, J.; Hancock, D.; Robbins, J.; Nattala, J.; Pavelsky, T.; Morrison, J.; Arp, C.; Jones, B. *ATLAS/ICESat-2 L3A Inland Water Surface Height, Version 1*; [Indicate subset used]; NASA National Snow and Ice Data Center Distributed Active Archive Center: Boulder, CO, USA, 2019.
66. Jasinski, M.; Stoll, J.; Hancock, D.; Robbins, J.; Nattala, J.; Pavelsky, T.; Morrison, J.; Arp, C.; Jones, B.; Ondrusek, M.; et al. *Algorithm Theoretical Basis Document (ATBD) for Inland Water Data Products, ATL13, Version 1*; Goddard Space Flight Center: Greenbelt, MD, USA, 2019; p. 89.
67. Magruder, L.; Neuenschwander, A.; Klotz, B. Digital terrain model elevation corrections using space-based imagery and ICESat-2 laser altimetry. *Remote Sens. Environ.* **2021**, *264*, 112621. [CrossRef]
68. Wang, C.; Zhu, X.; Nie, S.; Xi, X.; Li, D.; Zheng, W.; Chen, S. Ground elevation accuracy verification of ICESat-2 data: A case study in Alaska, USA. *Opt. Express* **2019**, *27*, 38168–38179. [CrossRef] [PubMed]
69. Bureau, Q.H. *Water Level Monitoring Data of Qinghai Lake in Xiashe Water Level Station*; TPDC: Beijing, China, 2019.
70. Zhang, G.; Xie, H.; Duan, S.; Tian, M.; Yi, D. Water level variation of Lake Qinghai from satellite and in situ measurements under climate change. *J. Appl. Remote Sens.* **2011**, *5*, 053532. [CrossRef]
71. Guo, H.; Jiao, W.; Yang, Y. The systematic difference and its distribution between the 1985 national height datum and the global quasigeoid. *Acta Geod. Et Cartogr. Sin.* **2004**, *33*, 100–104.
72. Carroll, M.L.; DiMiceli, C.M.; Townshend, J.; Sohlberg, R.A.; Elders, A.; Devadiga, S.; Sayer, A.; Levy, R. Development of an operational land water mask for MODIS Collection 6, and influence on downstream data products. *Int. J. Digit. Earth* **2017**, *10*, 207–218. [CrossRef]
73. JPL, N. *NASADEM Merged DEM Global 1 arc Second V001*; NASA EOSDIS Land Processes DAAC: Sioux Falls, SD, USA, 2020. [CrossRef]
74. Neumann, T.; Brenner, A.; Hancock, D.; Robbins, J.; Saba, J.; Harbeck, K.; Gibbons, A.; Lee, J.; Luthcke, S.; Rebold, T. *ATLAS/ICESat-2 L2A Global Geolocated Photon Data, Version 3*; NASA National Snow and Ice Data Center Distributed Active Archive Center: Boulder, CO, USA, 2020; Volume 10.
75. Yang, Y. Chinese geodetic coordinate system 2000. *Chin. Sci. Bull.* **2009**, *54*, 2714–2721. [CrossRef]
76. Leys, C.; Ley, C.; Klein, O.; Bernard, P.; Licata, L. Detecting outliers: Do not use standard deviation around the mean, use absolute deviation around the median. *J. Exp. Soc. Psychol.* **2013**, *49*, 764–766. [CrossRef]
77. Jiang, L.; Andersen, O.B.; Nielsen, K.; Zhang, G.; Bauer-Gottwein, P. Influence of local geoid variation on water surface elevation estimates derived from multi-mission altimetry for Lake Namco. *Remote Sens. Environ.* **2019**, *221*, 65–79. [CrossRef]
78. Blewitt, G.; Kreemer, C.; Hammond, W.C.; Gazeaux, J. MIDAS robust trend estimator for accurate GPS station velocities without step detection. *J. Geophys. Res. Solid Earth* **2016**, *121*, 2054–2068. [CrossRef]
79. Treichler, D.; Kääb, A.; Salzmann, N.; Xu, C.-Y. Recent glacier and lake changes in High Mountain Asia and their relation to precipitation changes. *Cryosphere* **2019**, *13*, 2977–3005. [CrossRef]
80. Yao, T.; Xue, Y.; Chen, D.; Chen, F.; Thompson, L.; Cui, P.; Koike, T.; Lau, W.K.-M.; Lettenmaier, D.; Mosbrugger, V. Recent third pole's rapid warming accompanies cryospheric melt and water cycle intensification and interactions between monsoon and environment: Multidisciplinary approach with observations, modeling, and analysis. *Bull. Am. Meteorol. Soc.* **2019**, *100*, 423–444. [CrossRef]
81. Fan, C.; Song, C.; Li, W.; Liu, K.; Cheng, J.; Fu, C.; Chen, T.; Ke, L.; Wang, J. What drives the rapid water-level recovery of the largest lake (Qinghai Lake) of China over the past half century? *J. Hydrol.* **2021**, *593*, 125921. [CrossRef]
82. Dong, H.; Song, Y. Shrinkage history of Lake Qinghai and causes during the last 52 years. In Proceedings of the 2011 International Symposium on Water Resource and Environmental Protection, Xi'an, China, 20–22 May 2011; pp. 446–449.
83. Luo, S.; Song, C.; Zhan, P.; Liu, K.; Chen, T.; Li, W.; Ke, L. Refined estimation of lake water level and storage changes on the Tibetan Plateau from ICESat/ICESat-2. *CATENA* **2021**, *200*, 105177. [CrossRef]
84. Xu, N.; Ma, Y.; Wei, Z.; Huang, C.; Li, G.; Zheng, H.; Wang, X.H. Satellite observed recent rising water levels of global lakes and reservoirs. *Environ. Res. Lett.* **2022**, *17*, 074013. [CrossRef]
85. Araki, S.; Deguchi, I. *Prediction of Wave Force Acting on Horizontal Plate above Still Water Level*; Department of Civil Engineering, Osaka University: Suita, Japan, 2012; pp. 1–2.
86. Haigh, I.D.; Nicholls, R.; Wells, N. A comparison of the main methods for estimating probabilities of extreme still water levels. *Coast. Eng.* **2010**, *57*, 838–849. [CrossRef]
87. Ryan, J.C.; Smith, L.C.; Cooley, S.W.; Pitcher, L.H.; Pavelsky, T.M. Global Characterization of Inland Water Reservoirs Using ICESat-2 Altimetry and Climate Reanalysis. *Geophys. Res. Lett.* **2020**, *47*, e2020GL088543. [CrossRef]